SERI/PR-8254-1-T1

AMORPHOUS THIN FILMS FOR SOLAR-CELL APPLICATIONS

Quarterly Report No. 1 for September 11—December 10, 1979

By
D. E. Carlson
R. S. Crandall
J. Dresner
B. Goldstein
J. J. Hanak
A. R. Moore
J. I. Pankove
H. A. Weakliem

December 1979

Work Performed Under Contract No. AC02-77CH00178

RCA Laboratories
Princeton, New Jersey

U.S. Department of Energy

Solar Energy

DISCLAIMER

DISCLAIMER

Available from the National Technical Information Service, U. S. Department of Commerce, Springfield, Virginia 22161.

Price: Paper Copy $7.00
Microfiche $3.50

SERI/PR-8254-1-T1
Distribution Category UC-63e

December 1979

Amorphous Thin Films for Solar-Cell Applications

Quarterly Report No. 1

For the Period 11 September 1979 to 10 December 1979

D. E. Carlson
R. S. Crandall
J. Dresner
B. Goldstein
J. J. Hanak
A. R. Moore
J. I. Pankove
H. A. Weakliem

RCA Laboratories
Princeton, New Jersey 08540

Prepared Under Subcontract No. XJ-9-8254
for the

Solar Energy Research Institute
A Division of Midwest Research Institute
1536 Cole Boulevard
Golden, Colorado 80401

THIS PAGE

WAS INTENTIONALLY

LEFT BLANK

PREFACE

This Quarterly Report covers the work performed by the Display and Energy Systems Research Laboratory of RCA Laboratories, Princeton, New Jersey, for the period 11 September 1979 to 10 December 1979 under Contract No. XJ-9-8254. The Laboratory Director is B. F Williams; D. E. Carlson is the Group Head and Project Scientist. The staff members and associate staff personnel who have contributed to the report, and their areas of specialization, are listed below.

D. E. Carlson R. W. Smith	dc Deposition of a-Si:H
*R. S. Crandall B. E. Tompkins	Photoconductive Gain, Drift Mobilities
*J. Dresner	Hall Effect
*B. Goldstein D. J. Szostak	Surface Studies
†J. J. Hanak J. P. Pellicane V. Korsun	rf Deposition of a-Si:H; Structures
*A. R. Moore G. R. Latham	Photoelectromagnetic Effect
†J. I. Pankove J. E. Berkeyheiser	Photoluminescence, Ion Implantation, Laser Annealing
*H. A. Weakliem A. V. Cafiero	rf Magnetron Deposition of a-Si:H

*Member of Technical Staff.

†Fellow.

THIS PAGE

WAS INTENTIONALLY

LEFT BLANK

SUMMARY

A new method for determining the drift mobility of majority carriers in doped a-Si:H is discussed in Section 2.0. This method examines the current transient introduced when majority carriers are extracted from a Schottky-barrier device. A drift mobility of 2.3×10^{-3} $cm^2 V^{-1} s^{-1}$ was determined for phosphorus-doped (0.2% PH_3) a-Si:H at 302 K.

Deposition and doping studies have been performed in an rf magnetron discharge system. Oxygen impurities have been reduced to ~400 ppm, but the material quality is still relatively poor, apparently due to the high concentration of SiH_2 and $(SiH_2)_n$ groups.

Mass spectroscopy has been used to show that the major impurities in the SiH_4 discharge occur at m/e values of 45, 47, and 49 at concentrations 10^{-4}-10^{-5} times that of the principal ion, SiH_3^+. The m/e = 49 peak may be due to the ion $SiH_3OH_2^+$, while the m/e = 45 peak appears to be associated with the diffusion pump oil.

Boron implantation of an i-n structure produces a p-i-n cell with an enhanced V_{oc} but reduced J_{sc} as compared to cells in a nonimplanted region. In this experiment the implanted and control regions were annealed in the presence of atomic hydrogen before the top Pt contact was deposited.

Laser annealing at power densities up to 60 MW/cm^2 (30-ns pulse) causes partial crystallization of the a-Si:H, but there are no significant changes in the photoluminescence spectrum or the hydrogen content.

In our final report [2], we showed surface photovoltage data with a peak at 0.62 eV. It is now apparent that this peak results from third-order diffraction lines of 1.86-eV photons. The surface photovoltage spectrum at room temperature of oxidized a-Si:H shows considerably smaller signals than that of a-Si:H with one monolayer of physisorbed oxygen.

The photo-Hall effect in undoped a-Si:H has been measured as a function of wavelength and temperature. The Hall mobility is $\sim$0.06-0.15 $cm^2V^{-1}s^{-1}$ (p-type) and is roughly independent of the wavelength of light. The Hall mobility does exhibit a complicated temperature dependence for temperatures greater than $\sim$400 K, and the behavior appears to depend on the thermal/illumination history of the sample.

The photoelectromagnetic spectrum for the short-circuit current has been used to estimate a hole diffusion length of $\sim$0.1-0.3 μm in undoped a-Si:H. A more accurate determination of the minority-carrier diffusion length is obtained from an analysis of the photoelectromagnetic open-circuit voltage, and then a value of $\sim$0.09 μm is obtained. This analysis also allows a determination of the hole mobility ($\sim 5.4 \times 10^{-3}$ $cm^2V^{-1}s^{-1}$), which is $\sim$7X smaller than the electron mobility in the same material.

Recently p-i-n cells have been fabricated with conversion efficiencies up to $\sim$4.5%. The automated testing system has been used to optimize the thickness of the p layer (using 0.6% B_2H_6 in SiH_4) at $\sim$8-26 nm and the n layer (using 1.3% PH_3 in SiH_4) at $\sim$40 nm. A series of different cermets has been investigated as contacts to the p layer, and efficiencies of $\gtrsim$4% were obtained with four cermets: Ir-Y_2O_3, Pt-Y_2O_3, Pt-TiO_2, and Pt-SiO_2. Preliminary studies show that relatively high values of J_{sc} may be obtained by illuminating a p-i-n cell through a top ITO contact on the n layer.

Both boron and phosphorus concentrations were found to vary inversely with rf power for doped a-Si:H films made in an rf capacitive discharge. A similar trend has been observed for phosphorus-doped films made in a dc(P) discharge.

Solar cells have also been fabricated with a-(Si,Ge):H alloys. While the addition of 2% GeH_4 to the SiH_4 discharge does not greatly affect V_{oc} at $T_s \simeq 200°C$, J_{sc} is reduced by $\sim$50%. Larger concentrations of GeH_4 reduce both V_{oc} and J_{sc} significantly. Thus, it does not appear that GeH_4 can serve to tailor the bandgap of a-Si:H solar cells.

The spectral response of i-n cells shows an increase in the long-wavelength response as the thickness of the i layer increases. In p-i-n cells, the short-wavelength response decreases as the thickness of the p layer increases. Modeling p-i-n cells by assuming a dead doped layer yields spectral response curves similar to those observed.

A study of the spectral dependence of the majority-carrier gain in a-Si:H solar cells has shown that the electron lifetime varies with excitation wavelength and is responsible for producing a peak in the photoconductivity spectra at $\sim$1.1 eV.

THIS PAGE

WAS INTENTIONALLY

LEFT BLANK

TABLE OF CONTENTS

TABLE OF CONTENTS (Continued)

LIST OF FIGURES

LIST OF TABLES

SECTION 1.0

INTRODUCTION

A review of the history of hydrogenated amorphous silicon (a-Si:H) and the a-Si:H solar cell can be found in Refs. 1 and 2. The present research program involves five tasks: theoretical modeling, deposition and doping studies, experimental methods for the characterization of a-Si:H, formation of solar-cell structures, and theoretical and experimental evaluation of solar-cell parameters.

In a separate program, researchers at RCA Laboratories are developing the technology to fabricate large-area ($\sim$40 cm^2) a-Si:H solar cells. This program has the objective of developing low-cost, large-area a-Si:H solar panels.

THIS PAGE

WAS INTENTIONALLY

LEFT BLANK

SECTION 2.0

THEORETICAL MODELING - DRIFT MOBILITIES FROM CURRENT TRANSIENTS

There are various methods to measure the drift mobility of charge carriers in electronic materials. Probably the most widely used is the time of flight method [3] in which a pulse of light or other high-energy radiation produces carriers at one face of a film of material. The pulse of carriers then drifts in the applied electric field to the opposite face of the film. The sign of the charge carrier depends on the polarity of the field. This technique works only when the dielectric relaxation time is longer than the transit time. If not, the charge packet is screened by the background charge. Another method that works only when the dielectric relaxation time is long is to measure transient space-charge injection current [4].

To measure the majority-carrier drift mobility in conducting materials we propose a new technique based on space-charge extraction. In this method one studies the change of the depletion width as majority carriers are extracted from a Schottky-barrier device. The shape of the accompanying current transient is analyzed to give the drift mobility.

The first part is an outline of the model calculation of depletion width widening during majority-carrier extraction. The second gives experimental evidence in support of the theory.

Consider an ideal Schottky barrier on an n-type semiconductor. The electron potential energy vs distance is shown in Fig. 2-1(a). This is the steady-state reverse-bias configuration with positive space charge of density (ρ) contained in the depletion width (W). The sample length is ℓ. If the bias (V_B) is changed so that the bands can just flatten, then electrons will flow from the bulk into the space-charge region and neutralize the positive charge shrinking the depletion width to zero. A further increase in bias would inject electron space charge.

If the bias is returned to its original value, electrons will leave the film. Since none can enter at the metal barrier contact (M_1), the space-charge region widens until it attains its original value (W), at which time the current has

decayed to zero. The characteristic time (τ_o) for this process is the transit time across the depletion width under the action of the average field (V_o/ℓ).

At some intermediate time the electron potential is as shown in Fig. 2-1(b). The boundary between the space-charge-field and neutral region is X_1. As electrons leave the space-charge region I, this boundary moves toward W. Its speed will be determined by such parameters as the mobility (μ), ρ, and the electric field distribution. Because the region II extending from X_1 to ℓ is neutral, the field (E_{II}) will be a constant of magnitude $V_1/(\ell - X_1)$ where V_1 is the potential at X_1. Since diffusion is neglected, the boundary between regions I and II will be sharp. The field (E_I) in the space-charge region I is nonuniform; it decreases linearly from the point 0 to X_1. It can be found by solving Poisson's equation subject to the boundary conditions: $V = -V_o$ at $X = 0$; $V = V_1$ at $X = X_1$.

The electron current in region II is ohmic and expressed by

$$J_{II} = -ne\mu E_{II} \tag{2-1}$$

where $ne = \rho$ and μ is the mobility characteristic of the charge flow through region II. If there is trapping, μ is the drift mobility. In region I the current is pure displacement current given by

$$J_I = \varepsilon \frac{dE_I}{dt} \tag{2-2}$$

where the dielectric constant is ε. By equating J_I with J_{II}, a differential equation for X_1 can be obtained. Its solution gives the time evolution of X_1 from 0 to W.

First, however, one must find the functional dependence of the fields E_I and E_{II} on X_1. This is accomplished by solving Poisson's equation in region I. Its first integral is

$$E_I = \frac{\rho}{\varepsilon} X + E_b(t) \tag{2-3a}$$

where the constant $E_b(t)$ is found by noting that the time integral of the displacement current (J_I) is just one half of the space-charge density remaining in region I. This condition gives

$$E_b(t) = -\frac{V_o}{W}\left[1 + \frac{X_1}{W}\right] \tag{2-3b}$$

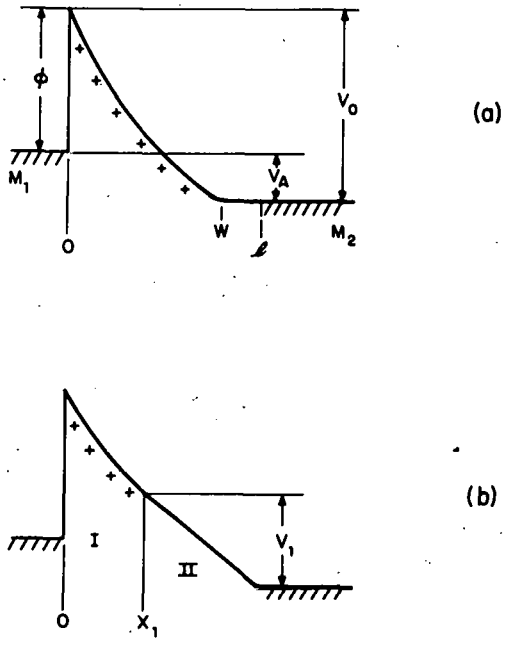

Figure 2-1. POTENTIAL ENERGY vs DISTANCE FOR SCHOTTKY-BARRIER STRUCTURES (a) AND (b). ϕ is barrier potential; M_1 and M_2 are barrier and ohmic contact metal, respectively; W is the depletion width, and ℓ is the sample thickness. V_o is the voltage drop across W, and V_A the applied voltage. I and II are the space charge and neutral region, respectively, separated by the point X_1.

where $W^2 = 2\,\varepsilon V_o/\rho$ gives the depletion width. Equation (2-3a) is now integrated to give V(X) and hence V_I. Then $E_{II} = \dfrac{V_1}{\ell - X_1}$

The ohmic current in II can be expressed in terms of the dimensionless variables $y = X_1/W$ and $a = W/\ell$ as

$$J_{II} = - J_o(1 - y)/(1 - ay) \quad ; \quad J_o = ne\mu\, V_o/\ell \tag{2-4}$$

In I the displacement current, based on Eqs. 2-2 and 2-3 is

$$J_I = - \frac{\varepsilon\, V_o}{W} \frac{dy}{dt} \tag{2-5}$$

Equations 2-4 and 2-5 yield a differential equation for y which, with the initial condition of y = 0 at t = 0, has the solution

$$t = \tau_c \quad (a - 1)\ \ln\ (1 - y) + ay \quad ; \quad \tau_c = \frac{\ell W}{2V_o\mu} \tag{2-6}$$

This relation between y and t can then be used with Eq. 2-4 for J_{II} to give an expression for the time dependence of the current. In general J_{II} can only be obtained by the numerical solution of Eq. 2-6. Nevertheless, inspection of Eq. 2-6 shows that at short times y increases linearly with t, and at long times y approaches unity exponentially.

To verify the above model calculation we made transient-current measurements on a 1.6-μm-thick amorphous silicon film produced by a dc glow discharge in silane containing 0.2% phosphine. The film was deposited on stainless steel at a temperature of about 300°C. After the film was removed from the growth system, a 50-Å platinum Schottky barrier was put on the silicon surface by electron-beam evaporation. The depletion width was determined by measuring the capacitance at 5×10^4 Hz, a value that is well below the dielectric relaxation frequency at room temperature. The capacitance exhibited the expected dependence on reverse bias for a classical Schottky barrier [5]. This behavior is required for the theory to be applicable.

For transient current measurements a negative dc bias (V_A) was applied to the Schottky-barrier contact to establish the depletion width W in the film. Then a positive voltage pulse of magnitude ΔV is applied to the Schottky barrier. The magnitude ΔV is chosen to just shrink the depletion width to zero. In the notation of Fig. 2-1 that shows $\Delta V = V_o$ this can be established in two ways: (1) by measuring the capacitance as a function of voltage; and (2) by observing that the space-charge injection current as a function of ΔV increases rapidly above the voltage necessary to collapse the depletion region. The pulse ΔV remains on for a time Δt sufficient to neutralize the space charge. This is on the order of 1 μs. After the termination of the pulse, the current transient due to electron extraction from the depletion region is observed. It is plotted in the inset of Fig. 2-2 for two different values of the applied bias. The current is detected by a magnetic current probe and amplified with a sampling scope. The two curves clearly show the effect of the dc bias on the decay time. If the current transient were due to capacitive charging of the metal contacts, the decay time would not depend on V_A.

In the body of Fig. 2-2 the solid curve is the normalized current vs normalized time from Eqs. 2-4 and 2-6. The points are data for two different values of

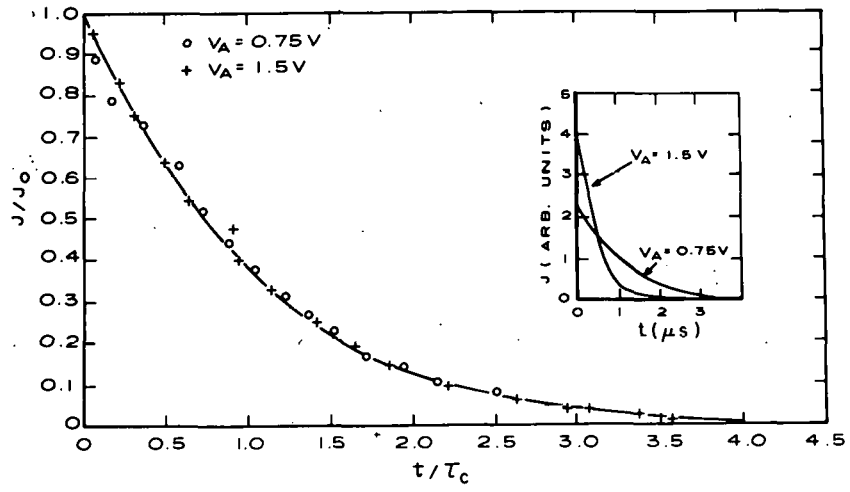

Figure 2-2. THE INSET IS THE CURRENT vs TIME MEASURED AT 302 K. THE SOLID CURVE IS THE NORMALIZED THEORETICAL CURVE. THE POINTS AND CIRCLES ARE THE DATA FROM THE INSET REPLOTTED ON THIS CURVE.

V_A. The associated J_o and τ_c were obtained by a least-squares fit to the theoretical curve. The agreement between theory and experiment is seen to be satisfactory.

Additional support to the model is given in Fig. 2-3 where J_o and $(\tau_c W)^{-1}$ are plotted vs V_A. These quantities vary linearly with V_A. The intercept is the built-in potential due to the Schottky barrier. From these data we find that $\mu = 2.3 \times 10^{-3}$ $cm^2V^{-1}s^{-1}$ at 302 K. This value is lower than has been previously reported for undoped and lightly doped a-Si:H [6,7]. The low mobility could be caused by the heavy phosphorus doping.

In Fig. 2-4 the logarithm of the drift mobility is plotted vs inverse temperature. The data fit a temperature-activated process with an activation energy (ΔE) of 0.13 eV. This would be consistent with a trap-limited drift mobility, as previously observed in a-Si:H [4,5]. In this heavily doped material, however, the activation energy is somewhat lower. At temperatures below ~270 K the data are less reliable because the time for emptying the shallow traps is becoming the order of the transit time across the depletion width. This precludes making low-temperature measurements to test if the mobility continues to be activated by a single activation energy.

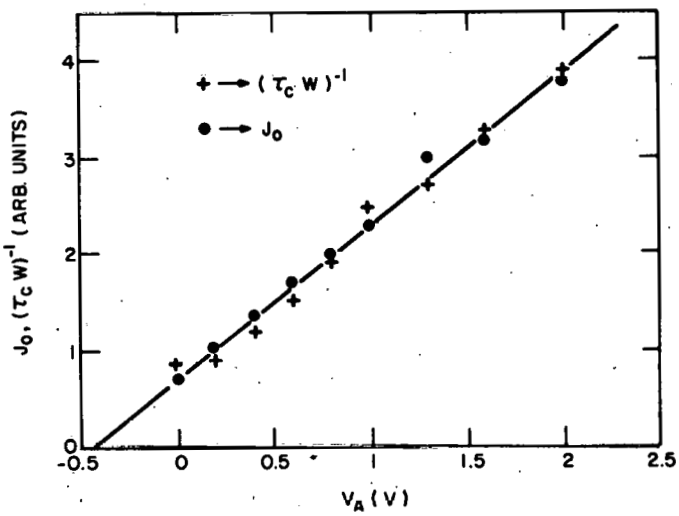

Figure 2-3. J_o AND $(\tau_c W_o)^{-1}$ vs V_A.

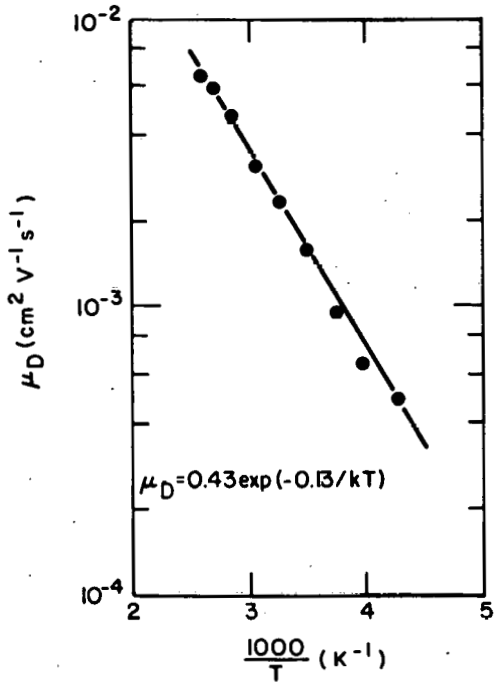

Figure 2-4. THE DRIFT MOBILITY vs 1/T FOR AN a-Si:H FILM DOPED WITH 0.2% PHOSPHORUS. The activation energy is 0.13 eV and the preexponential term in the mobility expression is 0.43 $cm^2 V^{-1} s^{-1}$.

SECTION 3.0

DEPOSITION AND DOPING STUDIES

3.1 rf MAGNETRON SYSTEM

3.1.1 Introduction

A study on doping a-Si:H with boron as a function of substrate temperature has been completed and a few Schottky-barrier cells consisting of Pt/undoped a-Si:H/n a-Si:H/stainless steel have been prepared at various stages during system modifications and improvements.

3.1.2. Boron Doping

Three films having different concentrations of boron in a-Si:H were prepared in a temperature gradient as part of a coordinated schedule. We find that the highest concentration of B used (1% B_2H_6 in silane) gave the highest conductivity. In all cases the conductivity was greatest for the hot end of the film. We should try boron doping at temperatures higher than the 330°C used previously. The magnitude of the conductivity in our most conductive sample is close to the values achieved in other glow-discharge systems.

3.1.3. Vacuum System Improvements

A new diffusion pump, Varian* VHS-6 equipped with a Mexican hat cold trap, has been installed on the magnetron/diode discharge system along with a new mechanical forepump.

We have made the necessary connections to enable the line-of-sight mass spectrometer to be used as a sensitive He leak detector. We have calibrated the sensitivity to be $\sim 5 \times 10^{-11}$ atm·cm^3/s, which compares favorably with high-quality He leak detectors. We have found and sealed several small leaks in the gas manifold and one leak in a weld joint of the stainless-steel chamber. This latter

*Varian-Extrion Corp., Gloucester, MA.

leak corresponded to a partial pressure of 3×10^{-8} Torr in the chamber, taking into account the known pumping speed of the system. We don't know if these small leaks adversely affect film properties; however, we are now assured that they are absent at least to a level below a partial pressure of 5×10^{-13} Torr.

3.1.4. Mass Spectroscopic Analysis of the rf Discharge

As we reported earlier [2], studies were begun on the analysis of positive ions produced in an rf discharge in silane. The dominant ion seen in a silane discharge is SiH_3^+; however, we also observe clusters of hydrides containing 2, 3, 4, 5, and 6 Si atoms. The relative concentration of multisilicon clusters compared with the single SiH_3^+ ion increases as the rf power decreases. For a given rf power, the single-ion intensity increases as the pressure decreases. Using the present location of the pinhole sampling aperture, we find that the positive ions detected do not sensitively depend on the discharge operating conditions, and that we shall have to improve the sampling configuration (i.e., move closer to the active-discharge region).

We have observed the persistent presence of unknown (impurity?) ions in a silane discharge having the values m/e = 45, 47, and 49. These ions have concentrations ranging from 10^{-5} to 10^{-4} that of the principal m/e = 31 ion due to SiH_3^+. In an attempt to identify these impurities, positive ion analysis was done on discharges containing mixtures of $SiH_4 + CO_2$ and $SiH_4 + N_2$. The effect of heating a substrate in a pure SiH_4 discharge was also investigated. These are the principal results of the analysis: the m/e = 49 peak is probably due to the ion $SiH_3OH_2^+$, and nitrogen is not involved in the 45, 47, and 49 mass peaks discussed earlier. The ion-molecule reactions in a mixture of SiH_4 and N_2 show that H_2O is preferentially detached from larger molecules and exists alone as the ion H_2O^+. That is to say, H_2O^+ (m/e = 18) is not present in a discharge of N_2 or SiH_4 alone; however, it appears strongly in a SiH_4/N_2 mixture, its concentration increasing as the nitrogen/silane ratio increases. We propose that an excited nitrogen molecule or ion collides with some $Si_xH_y(H_2O)_z^+$ species, causing a reaction that detaches a water molecule and thus produces free H_2O^+.

An experiment was performed in which a small amount of DC 704 diffusion pump oil was coated on the inside of a short stainless-steel cylinder, which in turn was

placed in front of the mass spectrograph aperture and exposed to a silane discharge. The results give strong evidence that the m/e = 45 ion results from a silane-siloxane (DC 704) reaction; the m/e = 47 and 49 ions, however, are unaffected. The ion m/e = 45 could be due to $SiOH^+$, but this identification has not been proven.

3.1.5. Future Plans

We shall attempt to do a mass analysis of the ions landing on a substrate plane in the dc proximity configuration, as a function of substrate temperature and bias. The necessary apparatus is being constructed. We will also continue the studies aimed at identifying the principal impurities present in the silane discharge.

3.2 HYDROGENATED BORON-IMPLANTED SCHOTTKY DIODES

The purpose of this experiment was to check if the conductivity of the p layer could be increased if the doping were produced by ion implantation. When this method had been tried earlier, the lack of success was attributed to the extensive damage induced by ion implantation. Thermal annealing is not suitable for a-Si:H because of the consequent loss of hydrogen. In the present experiment, to passivate the implantation-induced dangling bonds, the annealing treatment was done in the presence of atomic hydrogen.

The tests consisted in comparing the solar-cell characteristics of Pt/p-i-n/SS (stainless steel) with Schottky cells Pt/i-n/SS made on the same i-n/SS material. All the B-implanted cells exhibited a V_{oc} higher by 0.05-0.1 V than the unimplanted cells - a result consistent with a lowering of the Fermi level at the surface. Also, the series resistance decreased. However, the short circuit current was degraded by a factor of 2-4, so that the net effect was a drop in solar-cell efficiency. This poor overall performance is attributed to too thick a p layer - a problem that could be solved only by the use of implantation energies lower than those available.

THIS PAGE

WAS INTENTIONALLY

LEFT BLANK

SECTION 4.0

EXPERIMENTAL METHODS FOR CHARACTERIZING a-Si:H

4.1 LASER ANNEALING OF a-Si:H

In preparing the hydrogenated amorphous silicon, a-Si:H, by the glow-discharge decomposition of silane at a pressure of ~1 Torr, a capacitively coupled rf generator was used. A 10 Ω·cm n-type wafer of (111) crystalline silicon, c-Si, was used as a substrate maintained at 300°C during the decomposition. Laser annealing was performed with a single pulse from a Q-switched ruby laser at a power density of up to 60 MW/cm^2 in a 30-ns pulse.

4.1.1 Photoluminescence of Laser-Annealed a-Si:H

In the present study, different regions of the same layer of a-Si:H on c-Si were exposed at room temperature to a single pulse at seven different intensities of up to 60 MW/cm^2. The main photoluminescence characteristic of the seven regions is shown in Fig. 4-1. The most striking aspect of the emission spectrum is that the emission peak remains nearly constant, shifting to lower energy by about 0.01 eV with increasing annealing power. In several other series of laser annealing experiments, the emission peak did not shift by more than 0.02 eV. This result must be contrasted with observations made after thermal annealing that drives away hydrogen at temperatures above 350°C, whereupon the emission peak shifts to lower energy by at least 0.3 eV [8]. Therefore one would conclude that very little hydrogen has evolved from the laser-annealed specimen.

The emission intensity appears to drop at the higher laser powers. However, this drop in intensity can be readily accounted for without invoking a change in property: at the higher laser powers, the film is damaged, small patches of a-Si:H being ablated from the c-Si substrate. Thus the active area is reduced and the signal decreased accordingly. Note that the photoluminescence efficiency of c-Si substrate is much weaker than that of a-Si:H by several orders of magnitude, so that the substrate exposed through the holes in the film does not contribute to the luminescence signal.

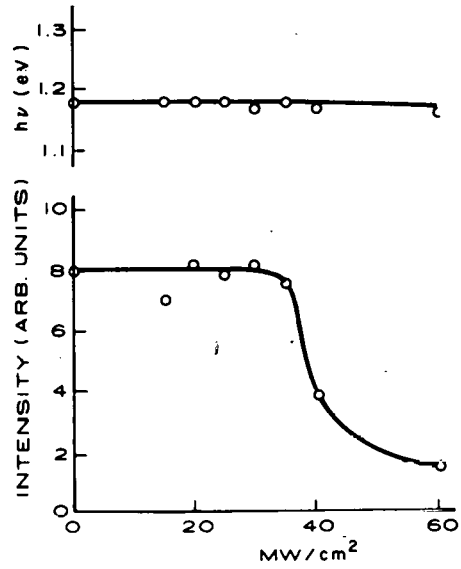

Figure 4-1. PHOTOLUMINESCENCE CHARACTERISTICS AT 78 K AS A FUNCTION OF THE ANNEALING POWER DENSITY. Upper curve: energy of the emission peak. Lower curve: intensity of the emission.

4.1.2 Hydrogen Concentration in Laser-Annealed a-Si:H

The hydrogen concentration was measured by secondary ion mass spectrometry (SIMS). Figure 4-2 compares the hydrogen profile of a laser-annealed sample with that of a nonannealed region. Although surface-charging problems with the nonannealed region induced a fluctuation in the hydrogen concentration data, the hydrogen concentration remained practically unchanged by laser annealing at 20 MW/cm^2. At the higher power levels, ablation damage reduces the effective area available for quantitative determination and reduces the hydrogen count (just as it did for the photoluminescence signal). Thus the SIMS measurements support the conclusion of negligible dehydrogenation arrived at from photoluminescence data.

4.1.3 Electron Diffraction of Laser-Annealed a-Si:H

Both the laser-annealed and nonannealed regions were examined by electron diffraction. In the nonannealed region, the diffuse pattern is typical of amorphous

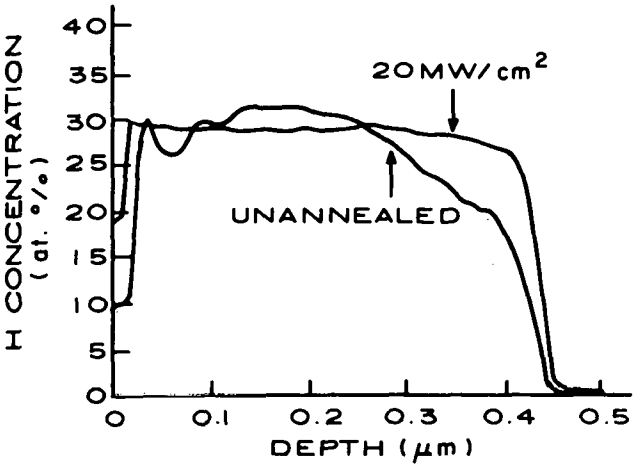

Figure 4-2. HYDROGEN CONCENTRATION PROFILES IN NONANNEALED AND IN LASER-ANNEALED a-Si:H.

material; but in the laser-annealed region, narrow bands appear which are characteristic of polycrystalline material. These diffraction patterns were scanned by a densitometer, and the resulting traces are reproduced in Fig. 4-3. The left-hand scale applies to the amorphous sample only. For the other two samples, the densitometer's controls were adjusted to enhance the visibility of the structure. Their structure corresponds to that of polycrystalline silicon. Since some diffuse background remains, one may conclude that at least part of the a-Si:H has crystallized. Unfortunately it is difficult to determine what fraction of the layer has crystallized, and therefore it is premature to conclude that the crystallized region still contains hydrogen. Yet, it is tempting to speculate on this possibility in view of other experiments showing that the impurity concentration in c-Si is not perturbed by laser annealing [9] and other work showing that amorphous silicon can be crystallized by laser annealing [10].

In conclusion, pulsed laser annealing of a layer of a-Si:H caused a partial crystallization of the material without appreciable loss of hydrogen from the film. However, more work is needed to determine the volumetric proportion of crystallized to amorphous material as a function of laser power density.

4.2 ELECTRON-BOMBARDMENT-INDUCED DAMAGE IN a-Si:H

It is known that a high-energy electron beam can damage a-Si:H. This has been reported in the study of electron-beam-induced conductivity [11], and is presently

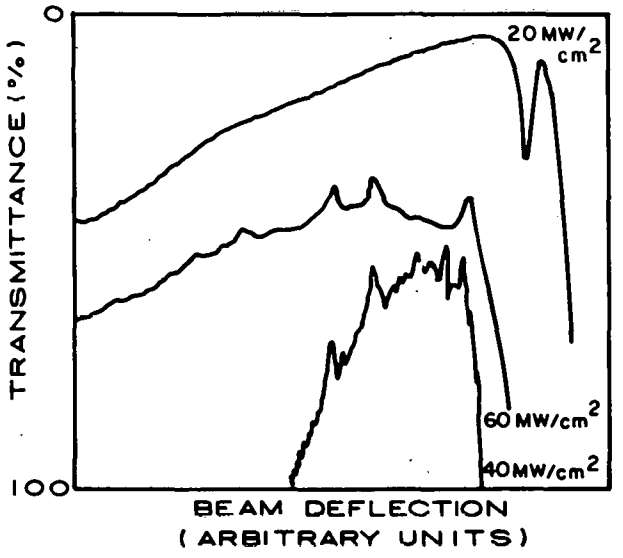

Figure 4-3. DENSITOMETER TRACES OF ELECTRON DIFFRACTION PATTERNS FOR SAMPLES EXPOSED TO THREE DIFFERENT LASER POWER DENSITIES. The left-hand scale applies to the upper trace only.

seen in secondary emission characteristics as well as in photoluminescence. A portion of a-Si:H on stainless steel was bombarded by a beam of 5-keV electrons depositing a charge density of 2 Coulombs/cm^2. In the bombarded region the luminescence intensity decreased by a factor of 25 at photon energies greater than 0.85 eV (Fig.4-4). Not much degradation occurred below 0.80 eV. After the sample was heated in vacuum at 300°C for 1/2 hour, the photoluminescence recovered to ~90% of the initial value. This indicates that almost no hydrogen was lost during electron bombardment. A SIMS analysis of another sample provided definitive support for this conclusion. Hence the damage may consist of broken Si-Si bonds. A subsequent exposure to atomic hydrogen at 300°C for 1/2 hour caused a complete recovery of the photoluminescence. Presumably, the last treatment replenished the hydrogen lost at the surface during the previous annealing in vacuum.

4.3 PHOTOLUMINESCENCE STUDIES

a-Si:H was deposited on one facet of a ZnSe prism. The photoluminescence was excited either by the customary frontal surface illumination or by illuminating the back surface of the a-Si:H film; in the latter method the excitation process

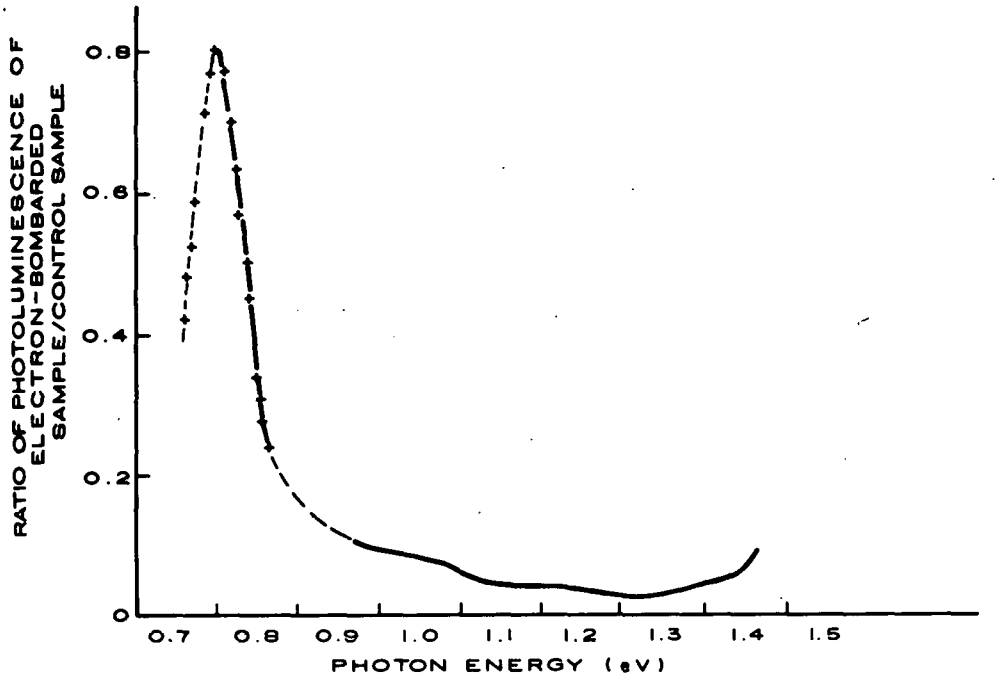

Figure 4-4. RATIO OF PHOTOLUMINESCENCE INTENSITIES OF ELECTRON-BEAM-DAMAGED AND -NONDAMAGED REGIONS AS A FUNCTION OF PHOTON ENERGY. The data below 0.80 eV is the ratio of two small signals.

benefits from multiple internal reflections. As shown in Fig. 4-5, in the presence of low-energy photons the multiple internal reflection mode is more efficient than frontal illumination. We are also planning to set up a facility for time-resolved luminescence spectroscopy.

The mapping of luminescence efficiency over the surface of a-Si:H is of great interest. The measurement is hampered by the need for scanning a large area at low temperature. We have built a new cold finger that allows scanning the luminescence intensity distribution over a 1/2-in. x 4-in. area. The scan could be mechanized eventually.

4.4 SURFACE STUDIES

4.4.1 Explanation of 0.62-eV Peak

A combination of fundamental difficulties in explaining the properties of the 0.62-eV surface photovoltage peak (SPV) reported in the Final Report of

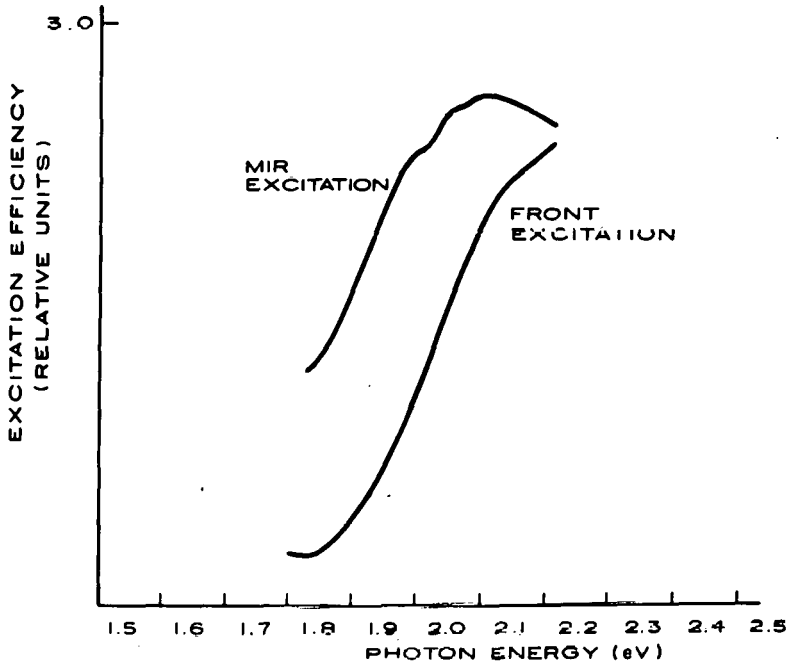

Figure 4-5. PHOTOLUMINESCENCE EXCITATION EFFICIENCY AS A FUNCTION OF PHOTON ENERGY FOR NORMAL FRONTAL ILLUMINATION AND FOR MULTIPLE INTERNAL REFLECTIONS.

November 1979 [see Ref. 2, Figs. 55 and 56], plus routine studies of SPV details at very low light levels, have led us to remeasure the transmission properties of the filters used in our work. By means of an optical stop not previously employed, (optical density of 2.0) transmission sensitivities were extended to 10^{-4}. As a result, we found that there was indeed a narrow window, centered at 1.9 eV and with a transmission of 1.5×10^{-4}, in the filters used for measuring the 0.62-eV SPV. Thus, the 0.62-eV peak actually appears to be a response due to third-order diffraction lines from the grating in our monochromatic light source that is passing through the 1.9-eV window; i.e., a SPV due not to 0.62-eV photons but to 1.86-eV photons. This one fact is able to explain all of the apparent anomalies of the 0.62-eV SPV; e.g., why the low-temperature 0.62-eV SPV response can be restored by heating to the same temperature as that which restores the 1.77-eV SPV response. No other region of the spectrum is so affected, so that all properties of the SPV at other wavelengths remain as reported.

4.4.2 Surface Photovoltage of Oxidized a-Si:H

Oxidation was carried out by exposing a-Si:H to an ambient of 5×10^{-4} Torr oxygen for several hours in the presence of ionizing sources. This produced

not only an oxygen line in the Auger spectrum 3-4 times larger than that corresponding to a monolayer of physisorbed oxygen, but also a Si line almost completely in the oxide state (no such oxide-state Si was seen with a monolayer of physisorbed oxygen). The basic SPV spectra at room temperature and at -168°C of oxidized a-Si:H are shown in Fig. 4-6. Note that while the SPV of the O_2-physisorbed surface, curve (b) Fig. 4-6, was similar in shape to that of the clean surface, the SPV of the oxidized surface is considerably different. The zero response at room temperature between 1.6 and 2.0 eV was found to be due not to a total absence of any SPV signal, but rather to two (or more) SPV transitions of opposite polarity. In addition, the rise and decay times of the SPV at -168°C are even slower than those for the clean surface. Only the response above 2.0 eV has the same characteristics as those for the clean and physisorbed surface, as seen in Fig. 4-6. The situation appears to be very complicated, and we suggest that this may be due not only to the presence of a different material at the surface (i.e., SiO_2), but also to the fact that we may be seeing the results of both interface states (Si-SiO_2) and free-surface states (SiO_2) of a large-bandgap material. Initial attempts at detailed measurements intended to separate out the effects of interface states and surface states are not encouraging.

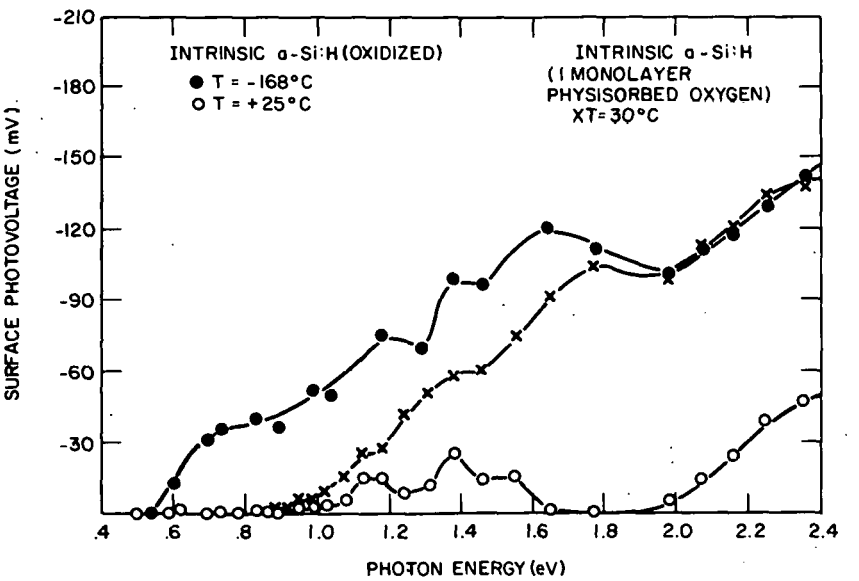

Figure 4-6. SURFACE PHOTOVOLTAGE AS A FUNCTION OF PHOTON ENERGY FOR OXIDIZED a-Si:H AND a-Si:H WITH ONE MONOLAYER OF PHYSISORBED OXYGEN

4.5 HALL EFFECT IN UNDOPED a-Si:H

A central idea in studying charge transport in an amorphous semiconductor such as a-Si:H is that there exists a bandgap whose limits are set by "mobility edges"; these mobility edges are believed to separate localized from extended states. In a recent review paper [12], Weiser has pointed out that there is no experimental evidence for the existence of a mobility edge for any amorphous semiconductor except a-Si:H. For that material, the evidence consists only of one interpretation of changes in the slope of conductivity vs reciprocal temperature. Such an interpretation has been used by one major group of investigators, the "Dundee School" [13-15]. They postulate a two-band model for conduction by electrons; below 250 K conduction takes place by thermally assisted hoppings between states in the band tails, while above 250 K the electron conduction is mostly in the extended states, where the mobility should be in the range 1-10 $cm^2V^{-1}s^{-1}$ and independent of temperature. The model consistently fits with their experimental results of conductivity as a function of temperature.

The measurements of drift mobility by several investigators can also fit this model [7,13]; if one combines these with photoconductivity data by the classical model [16], one would predict mobilities in the extended states of $\mu_o \sim 20$ for electrons and $\mu_o \sim 5$ for holes. The model has also been used to analyze the Hall-mobility data for lightly and heavily doped a-Si:H.

Another major group of researchers, the "Marburg School" [17-19], has arrived at a somewhat different picture by analyzing the behavior of the conductivity σ together with that of the thermoelectric power S. They conclude that the changes in the slopes of $\sigma(T)$ and $S(T)$ are due to a statistical shift of the Fermi level and that the mode of conduction remains the same from 200 to 600 K with μ thermally activated in this range. From their data they derive an expression $\mu \sim (4/kT) \exp(-0.1/kT)$, yielding $\mu \sim 4$ $cm^2V^{-1}s^{-1}$ at room temperature. No mobility gap is involved in this picture.

We are trying to measure the Hall mobility in undoped a-Si:H for carriers we can identify as being in the extended states and perhaps to distinguish between the two models. So far, Hall measurements have been made only in lightly and heavily doped samples [14,17]. Because of the high resistivity of the most lightly doped

specimen, only a narrow temperature range has been investigated. It was found that $\mu_H \sim 0.1$, with a reversed sign and generally temperature independent. If there exist two modes of conduction with widely different mobilities, one might be able to shift the relative electron population of the two levels by intense illumination and, as long as the photocurrent is large compared to the dark current, one might reach a temperature where the high-mobility mode dominates the Hall effect; one might then expect to find an abrupt change in sign or magnitude of μ. The question remains as to what quantity is measured by the Hall effect in a-Si:H. For hopping transport in localized states in the band tails one will find μ reversed in sign and thermally activated [14,20]. For diffusive transport in states just above the mobility edge, where $\mu \gtrsim 1\text{-}10$ (mean free path $\gtrsim$ 2 atomic spacings) Friedman [20] has calculated that $\mu_H \sim 0.1\ \mu$; it would be reversed in sign and temperature insensitive.

An apparatus has been built that is capable of measuring samples with a resistance exceeding $10^{11}\ \Omega$ and with circuitry to mimimize the effect of the potential drifts that are common to insulating photoconductors. It was found that the response time upon changes of magnetic field can be very long (as much as 100 s), particularly above 100°C. This was attributed to the large density of deep traps in this material. It was found necessary to control the temperature to better than 1 K and to allow more than 30 min to stabilize the sample upon changing the temperature. Also the noise level is large enough so that the Hall voltage must often be obtained by graphical integration of the data.

Two reliable results have been obtained so far:

(a) At room temperature (28°C) μ_H has been measured as a function of λ by combinations of broad-band filters ranging from $\lambda = 0.34\text{-}0.60\ \mu m$ to $\lambda > 1.04\ \mu m$; μ_H was p type and varied unsystematically between 0.06 and 0.15 $cm^2V^{-1}s^{-1}$. The conductivity varied between 3×10^{-8} and $1 \times 10^{-5}\ \Omega^{-1}cm^{-1}$. The optical bandgap was measured to be 1.62 eV (0.77 μm). Thus all wavelengths of light excite electrons to the same conducting state. The same result was recently deduced by R. S. Crandall from analysis of photoconductivity in solar cells (see Section 6.2).

(b) μ_H was measured as a function of temperature under an illumination of $\tilde{\sim}$ 100 mW/cm^2 in the λ range of 0.59-0.70 μm. For samples annealed at about 200°C, μ_H was p type after the sample was stabilized at a constant temperature. μ_H remained approximately at 0.1 $cm^2V^{-1}s^{-1}$ from 300 to 400 K, then rose in the temperature range 400-550 K with an activation energy of 0.12 eV. In the narrow temperature range 480-540 K, n-type signals were found in two runs. Since in these runs the samples had not been stabilized at constant temperature, this may have been a transient effect caused by the hole traps being emptied. When the sample had been light-soaked (by intense illumination for several days by a mercury arc lamp), μ_H was approximately 0.1 $cm^2V^{-1}s^{-1}$ in the range 208-450 K.

4.6 PHOTOMAGNETOELECTRIC EFFECT IN a-Si:H

In the photomagnetoelectric effect (PME) hole-electron pairs are created by light and drift by diffusion in a magnetic field. The resultant current or voltage at right angles to the drift direction and the magnetic field is a measure of the motion of the minority carrier. In a-Si:H conventional photoconductivity or drift mobility, measurements yield information about majority carriers. Yet in solar cells, minority-carrier motion is essential. The PME method should make it possible to characterize minority carriers in material without junctions or applied fields.

The most important advance in this quarter has been the confidence we have gained in the measurement. The measured PME current is very small, 10^{-13} to 10^{-14} A, and many confusing side effects are possible. We are now convinced that the measurement is real and will lead to interesting results, especially in regard to minority-carrier parameters.

We have measured the spectral distribution of the short-circuit PME current and the photoconductive (PC) current. Both spectra cut off as we proceed from the blue into the red end of the spectrum. The PME spectrum falls more rapidly than the PC spectrum. The fundamental reason for this is that the PME current depends on a diffusion current, hence a concentration gradient. The characteristic parameter defining the fall-off is αL, where α is the absorption coefficient and L is the minority-carrier diffusion length. Fall-off occurs when $\alpha L \leq 1$. On the other hand, the PC current is controlled by the total number of carriers

(mainly majority) generated by the absorbed light, independent of their spatial distribution. The characteristic parameter defining the fall-off is $\alpha\ell$, where ℓ is the sample thickness. The PC current decreases when $\alpha\ell \leq 1$. Since $\ell/L \gg 1$, i.e., the diffusion length is short, αL becomes <1 where $\alpha\ell$ is still large. The result is that the PME current falls more rapidly than the PC current as α is decreased by going to longer wavelengths. By fitting the experimental PME spectrum at long wavelengths to a theoretical form for the fall-off, the value of L can be estimated. We obtain values from 0.1 to 0.3 μm. This agrees with Wronski's original estimate based on collection efficiency measurements in solar-cell structures, and is longer than Staebler's more recent estimate. No doubt there is considerable variation in this parameter with structural perfection, or lack of it, in various preparations. Indeed, that was one of the reasons for undertaking the PME measurement, for it provides one of the few methods for obtaining the minority-carrier diffusion length.

One of the difficulties in fitting the short-circuit PME current to the theoretical form is that the experimentally observed current falls off at the blue end of the spectrum as well, a situation not predicted by PME diffusion theory. We believe this is due to either surface or volume boundary conditions different from those ordinarily assumed. A way out of this problem is to measure the open-circuit voltage instead of the short-circuit current. In general, for any linear current generator, the open-circuit voltage is the short-circuit current divided by the conductance. Because the photoconductance also falls off in the blue end of the spectrum, the ratio of I_{sc} to conductance remains constant. In particular, PME theory predicts that at light levels at which the photoconductivity dominates the dark current, the PME open-circuit voltage should become independent of light, intensity (i.e., it should saturate). This saturation has been clearly observed through the entire visible spectrum. A plot of the saturated value of the PME open-circuit voltage (V_{PME}^{oc}) vs α, the absorption coefficient at a given wavelength, follows the theoretical form quite closely. From this plot, and variations of it, one can obtain the value of the diffusion length (L), the ratio of the ambipolar diffusion coefficient to the diffusion length (D/L), and the normalized surface recombination velocity (SL/D). The accuracy of the V_{PME}^{oc} method of obtaining L is much better than that of the I_{PME}^{sc} method, first because it follows the theoretical formulation over the whole visible spectrum and second because it does not require the absolute or even the relative light intensity.

All that is required is that the V_{PME}^{oc} saturates. Combined with the I_{PME}^{sc} data we obtain the following for the sample of undoped dc discharge material under investigation: $L = 0.09\ \mu m$, $D/L = 15\ cm/s$, $D = 1.35 \times 10^{-4}\ cm^2 s^{-1}$, $\mu_p = 5.4 \times 10^{-3}\ cm^2 V^{-1} s^{-1}$, $\mu_n = 3.7 \times 10^{-2}\ cm^2 V^{-1} s^{-1}$, $\mu_n/\mu_p = 6.8$, and $SL/D \cong 0.3$. Thus it appears that all the important transport parameters of a-Si:H can be estimated by the PME method.

Finally, the sign of the PME effect is of interest. Based on comparison with a sample of germanium, the sign is found to be normal; i.e., holes and electrons are deflected in the expected directions by the magnetic field. Two special crystalline Si samples were prepared, one n type, one p type; these were used to make certain that the comparison holds. The reason this result is unusual is that the Dundee group has found the sign of the Hall effect in unilluminated doped a-Si:H to be opposite to that expected for normal n- and p-type materials. The experimental and theoretical ramifications of this dilemma cannot be foreseen.

SECTION 5

FORMATION OF SOLAR-CELL STRUCTURES

5.1 OPTIMIZATION OF MATERIALS AND STRUCTURES IN a-Si:H SOLAR CELLS

5.1.1 Increased Efficiency in p-i-n a-Si:H Cell

We have fabricated a p-i-n solar cell yielding efficiencies (η) of up to 4.46% in simulated AM1 sunlight and 4.15% in natural sunlight on cell areas of 2.5 mm^2. The cell structure consisted of glass/indium-tin oxide(ITO)/Ir-Y_2O_3 cermet/ p-i-n a-Si:H/Ti, which was illuminated through the glass. This increase in η has been the result of systematic optimization of materials parameters and deposition conditions described below. The I-V curve taken in AM1 sunlight is shown in Fig. 5-1.

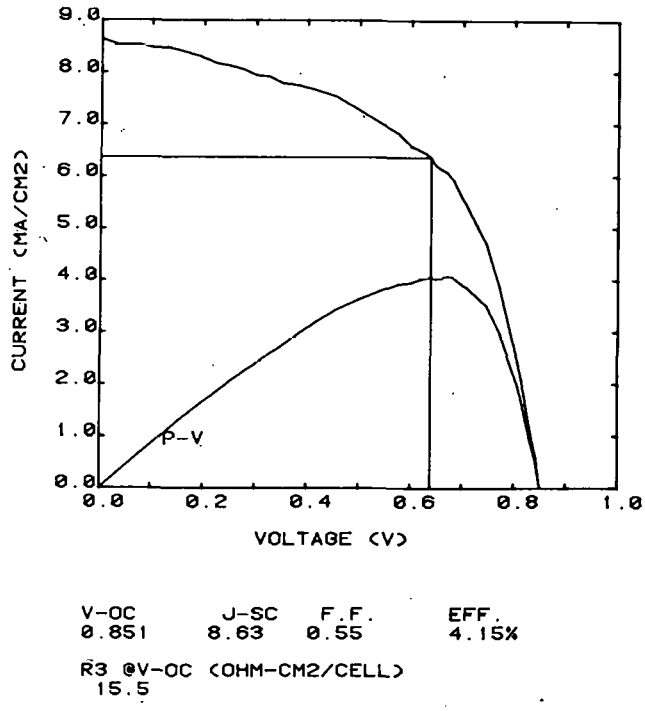

Figure 5-1. THE PERFORMANCE OF A p-i-n a-Si:H CELL ILLUMINATED THROUGH THE GLASS SUBSTRATE. Area, 2.5 mm^2; illumination, 0.98 AM1.

5.1.2 Optimization of p- and n-Layer Thicknesses at Higher Dopant Concentrations

In our previous report a set of optimized parameters was given for the fabrication of p-i-n a-Si:H solar cells. That set of data was obtained for relatively

low dopant concentrations (of the order of 10^{-3}) and at relatively high rf power ($\sim$0.9 W/cm^2). Low boron concentration required relatively large thicknesses, and this has led to low quantum efficiencies (QE) at short wavelengths. Increased dopant concentration holds the promise of smaller p-layer thicknesses as well as higher doped-layer conductivities leading to higher fill factors. This meant, however, that the thicknesses of the a-Si:H layers had to be optimized again for the higher dopant levels.

A solar-cell structure consisting of glass/ITO/Pt-SiO_2 cermet/p-i-n a-Si:H/Ti was made, having graded thicknesses of the p layer from 0 to 800 Å and of the n layer, at right angles, from 0 to 1030 Å. A constant i-layer thickness of $\sim$6000 Å was used. The dopant levels were 0.6% B_2H_6/SiH_4 and 1.3% PH_3/SiH_4. The p and i layers were deposited at a low rf power (0.12 and 0.09 W/cm^2) and the n layer at a higher power (0.6 W/cm^2); T_s was 200°C. The sample was measured under $\sim$AM1 illumination and contour plots were made of the performance parameters.

The more significant observations are the following: maximum V_{oc} ($\sim$800 mV) was reached at a thickness of 160 Å of the p layer as opposed to 360 Å for lower (1×10^{-3}) boron doping. The contribution to the V_{oc} by the p layer was only 100 mV, probably because at "zero" thickness there was a very thin p layer present. Maximum J_{sc} occurred at "zero" thickness of the p layer, but the J_{sc} variation with thickness was smooth, as before. The n layer contributed 250 mV to the V_{oc}: maximum V_{oc} and J_{sc} were reached at $\sim$310 Å of the n layer. The series resistance was lowered drastically by the n layer, reaching a low plateau also at 310 Å. Optimized parameters based on efficiency will be given after the next section. Contour plots of V_{oc}, J_{sc}, FF, η, and series resistance R_4 at 1-V forward bias are shown in Figs. 5-2 to 5-6, respectively.

5.1.3 Optimization of the i- and n-Layer Thicknesses at Higher Dopant Concentrations

A solar-cell structure consisting of glass/ITO/Pt-SiO_2 cermet/i-n a-Si:H/Ti was made, having graded thicknesses of the i layer from 0 to 8000 Å and of the i layer at right angles, from 0 to 780 Å. The rf power for the i layer and the n layer was 0.09 and 0.12 W/cm^2, respectively, and the T_s used was 220°C.

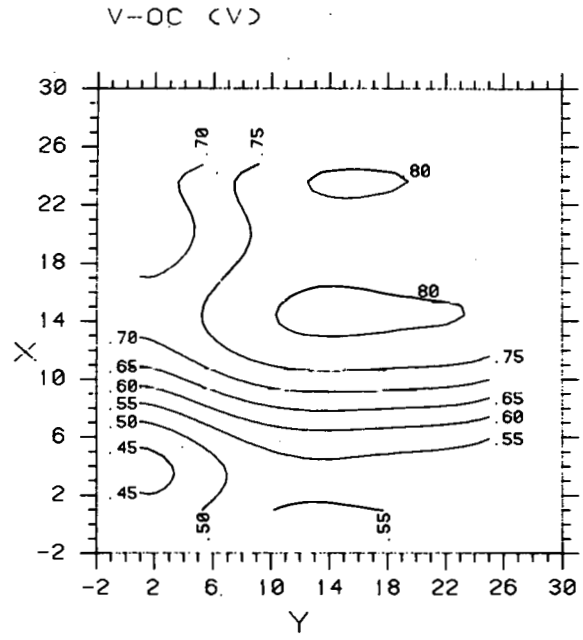

Figure 5-2. CONTOURS V_{oc} (V) OF p-i-n CELLS HAVING THE p LAYER GRADED IN THE Y DIRECTION (Y = 1-7, d(p) $\sim$ 0 nm; Y = 7-25, d(p) $\sim$ 0 to 80 nm) AND THE n LAYER GRADED IN THE X DIRECTION (X = 1-7, d(n) $\sim$ 0 nm; X = 7-25, d(n) $\sim$ 0 to 103 nm). The i-layer thickness is 600 nm; cell area $\sim$ 2.5 mm^2; simulated AM1 illumination through the glass substrate.

Contour plots of the AM1 solar-cell performance indicate a V_{oc} of 250 mV for the Pt-SiO_2/i a-Si:H Schottky diode without the n layer, and 500 mV with the n layer. A very large decrease of the series resistance takes place with the addition of the n layer; at 1-V forward bias R_4 drops from 500 to 2 $\Omega \cdot cm^2$. J_{sc} is dominated primarily by the i-layer thickness, but is also affected by the n thickness. J_{sc} was still increasing slowly at an i-layer thickness of 8000 Å. The fill factor (FF) increased drastically with increasing n-layer thickness, but also increased inversely with the i-layer thickness.

Based on the new results for the p-i-n and i-n cells in which the thicknesses were graded, the optimum thicknesses for the three layers are those given in Table 5-1 (for cells illuminated through the p layer).

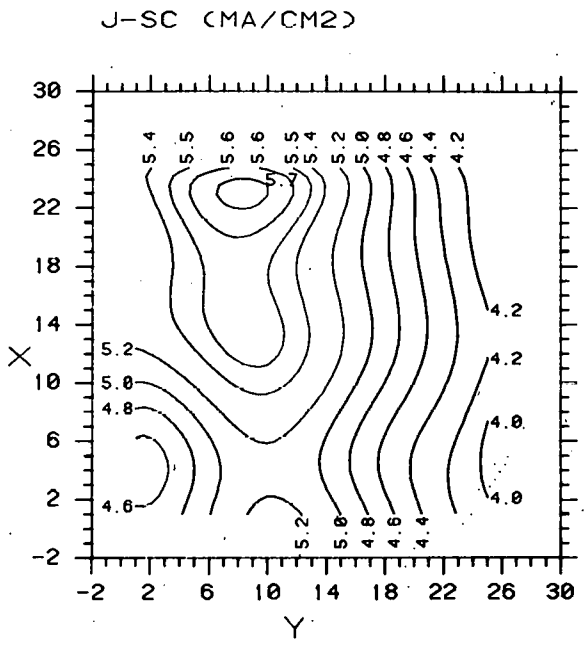

Figure 5-3. CONTOURS OF J_{sc} (mA/cm^2) FOR CELLS DESCRIBED IN THE CAPTION FOR FIG. 5-2.

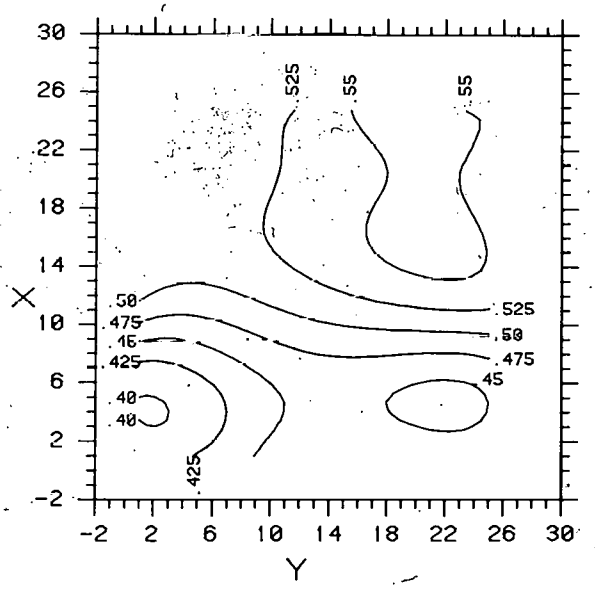

Figure 5-4. CONTOURS OF THE FILL FACTOR FOR CELLS DESCRIBED IN THE CAPTION FOR FIG. 5-2.

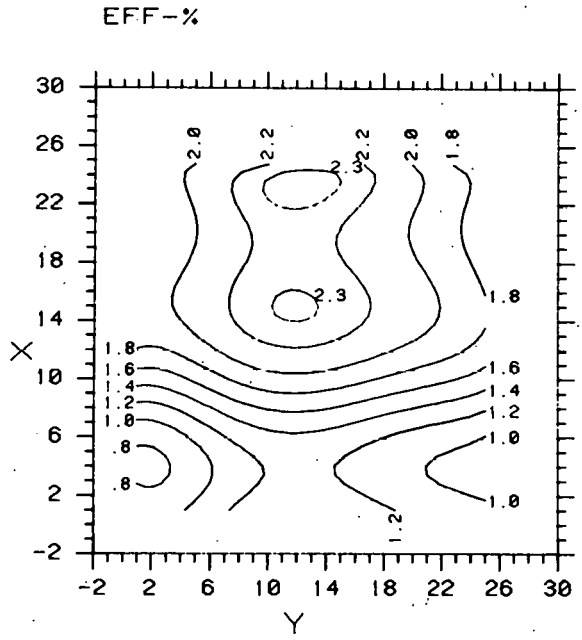

Figure 5-5. CONTOURS OF CELL EFFICIENCY (%) FOR CELLS DESCRIBED IN THE CAPTION FOR FIG. 5-2.

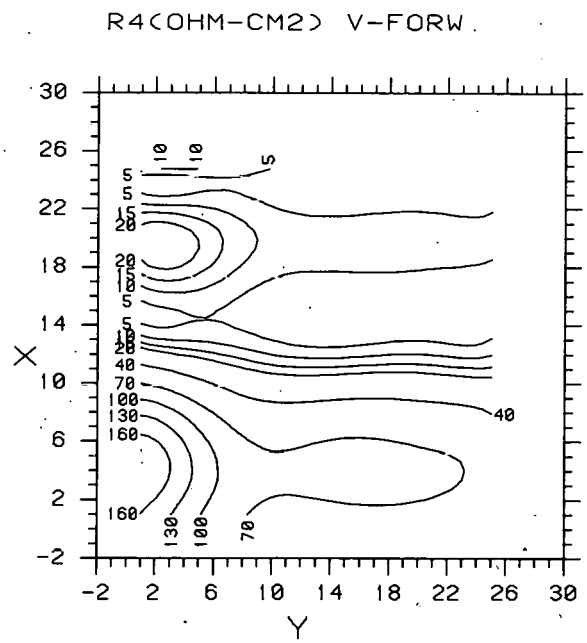

Figure 5-6. CONTOURS OF SERIES RESISTANCE R_4 ($\Omega \cdot cm^2$) at 1 V FORWARD BIAS FOR CELLS DESCRIBED IN THE CAPTION FOR FIG. 5-2.

Table 5-1. RECOMMENDED THICKNESSES FOR a-Si:H LAYERS FOR SOLAR CELLS

Layer	Thickness (Å)
p	75-260
i	≥8000
n	≥360

The contour plots of V_{oc}, J_{sc}, FF, η, and R_4 are shown in Figs. 5-7 to 5-11, respectively.

A striking difference has been observed between the IV curves of cells with and without the n layer under illumination as shown in Figs. 5-12(a) and 5-12(b), respectively. The absence of the n layer leads to the formation of an opposing Schottky contact, i a-Si:H/Ti, which lowers the net V_{oc} and creates the second hump in the forward-bias region of the IV curve.

5.1.4 Contributions to V_{oc} by Various Junctions

The difference in the maximum V_{oc} of the i-n sample (500 mV) and the preceding p-i-n cells (800 mV) indicates that the contribution by the p layer to V_{oc} is greater than 300 mV. A list of tentative contributions to the V_{oc} by three different junctions in the inverted p-i-n structure is given in Table 5-2.

5.1.5 Improved Cermets for Contacts to p Layer

We carried out a study of different cermets for contacts to the p a-Si:H layers. We cosputtered cermets graded in metal content from ~6 to ~35 vol %, using metals differing in work function, ϕ, and insulators differing in bandgap, E_g. A p-i-n/Ti solar-cell structure was deposited over the cermets, based on the data shown in Table 5-1. The cermets yielding the highest V_{oc} and η consist of high ϕ metals and intermediate E_g insulators (>5 and 3.3-6 eV, respectively). The cermets in the order of efficiencies obtained are listed in Table 5-3. It was in this series of tests that the highest efficiency of 4.46% to date for this cell structure was obtained. A simulated AM1 sunlight source was used.

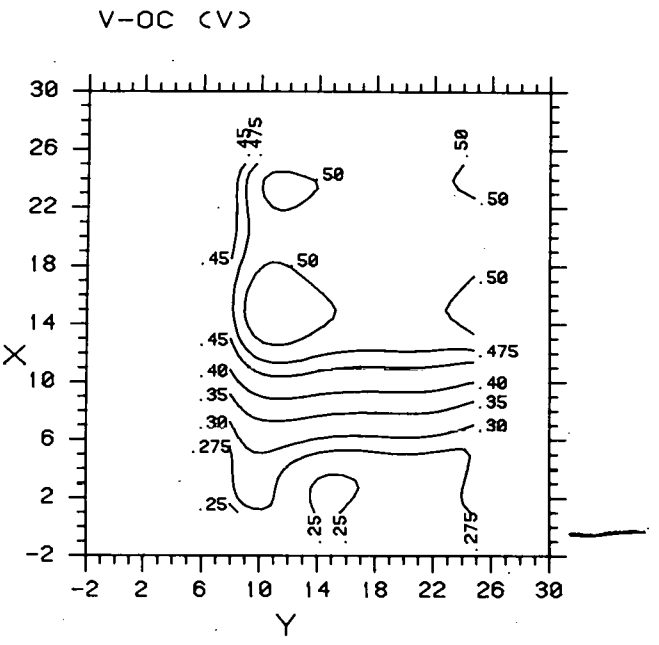

Figure 5-7. CONTOURS OF V_{oc} (V) OF i-n CELLS HAVING THE i LAYER GRADED IN THE Y DIRECTION (Y = 1-6, d(i) ≃ 0 nm; Y = 6-25, d(i) ≃ 0 to 800 nm) AND THE n LAYER GRADED IN THE X DIRECTION (X = 1-9, d(n) ≃ 0 nm; X = 9-25, d(n) ≃ 0 to 78 nm). Cell area = 25 mm^2; simulated AM1 illumination through the glass substrate.

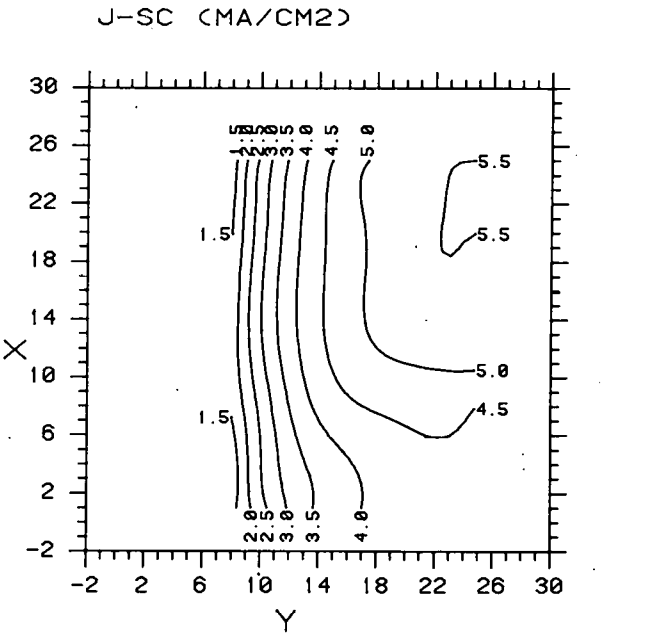

Figure 5-8. CONTOURS OF J_{sc} (mA/cm^2) FOR CELLS DESCRIBED IN THE CAPTION FOR FIG. 5-7.

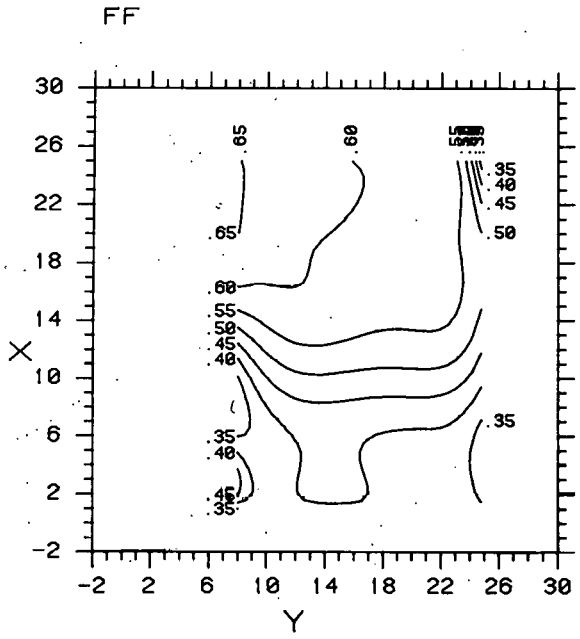

Figure 5-9. CONTOURS OF THE FILL FACTOR FOR CELLS DESCRIBED IN THE CAPTION FOR FIG. 5-7.

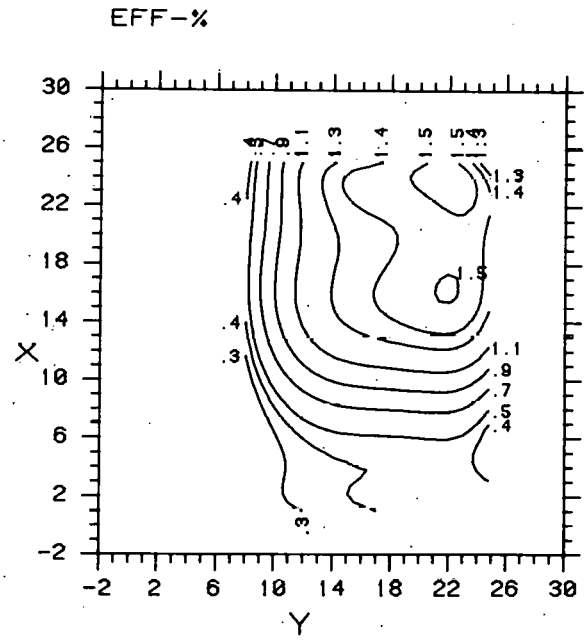

Figure 5-10. CONTOURS OF CELL EFFICIENCY (%) FOR CELLS DESCRIBED IN THE CAPTION FOR FIG. 5-7.

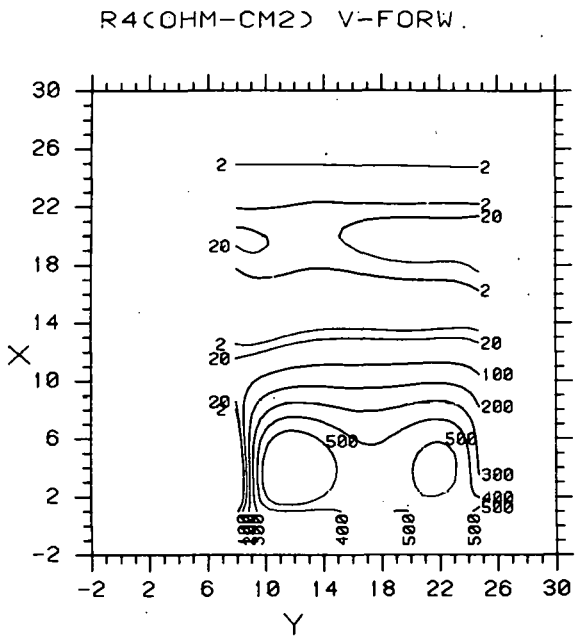

Figure 5-11. CONTOURS OF SERIES RESISTANCE R_4 ($\Omega \cdot cm^2$) AT 1-V FORWARD BIAS FOR CELLS DESCRIBED IN THE CAPTION FOR FIG. 5-7.

5.1.6 Front and Back Illumination of p-i-n a-Si:H Solar Cells

Inverted p-i-n cells having the structure of glass substrate/ITO/Pt-SiO_2 cermet/ p-i-n a-Si:H/back electrode were fabricated. Two kinds of back electrodes were used, including thick sputtered Ti, and 1/4-wave ITO on the bare n layer. The back ITO was e-beam evaporated at a 45° angle. When annealed, the back ITO had a sheet resistivity exceeding 1000 Ω/□. The p- and n-layer thicknesses* were about 700 Å and the i-layer thickness was 6000 Å. Front (through glass) and back (through film) illumination was used to evaluate the cell performance shown in Table 5-4.

The low fill factor for the ITO back electrode is primarily due to the high sheet resistivity, but also to a back barrier; this is evident from the presence of a second hump in the far-forward bias of the IV curve. [In a similar sample, which has, however, a thin (20 Å) sputtered Ti between the n and the ITO layers, no barrier was evident.]

*Thickness-graded sample was used.

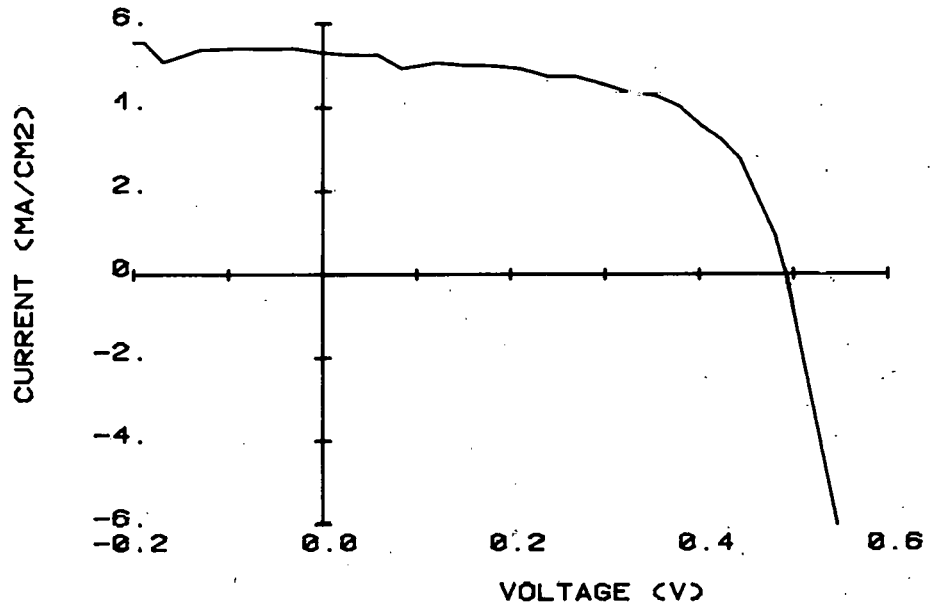

(a)

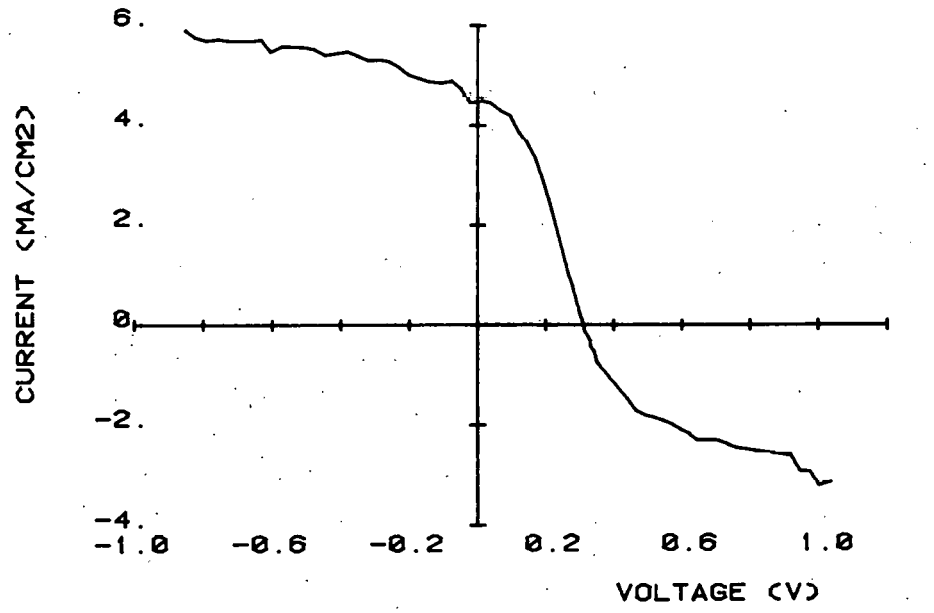

(b)

Figure 5-12. (a) I-V CURVE FOR A CELL, ITO/Pt-SiO_2 cermet/i a-Si:H/n a-Si:H/Ti; simulated AM1 illumination. (b) I-V CURVE FOR A CELL, ITO/Pt-SiO_2 cermet/i a-Si:H/Ti; simulated AM1 illumination.

Table 5-2. CONTRIBUTION TO V_{oc} BY DIFFERENT JUNCTIONS IN THE INVERTED p-i-n a-Si:H CELL

Junction	V_{oc} (mV)
Pt-SiO_2/p a-Si:H	220
p/i a-Si:H	>300
i/n a-Si:H	250

Table 5-3. COMPARISON OF SOLAR-CELL PERFORMANCE OF p-i-n a-Si:H STRUCTURES CONTAINING DIFFERENT CERMETS

Cermet	V_{oc} (mV)	J_{sc} (mA/cm^2)	FF	η (%)	ϕ of M (eV)	E_g of I (eV)
Ir-Y_2O_3	827	9.66	0.558	4.46	5.5	5.6
Pt-Y_2O_3	824	9.16	0.590	4.43	5.6	5.6
Pt-TiO_2	797	9.0	0.558	4.0	5.6	3.3
Pt-SiO_2	798	8.80	0.564	3.94	5.6	8.0
Ir-SiO_2	794	8.18	0.559	3.63	5.5	8.0
Mo-SiO_2	697	9.0	0.526	3.3	4.2	8.0
Ti-SiO_2	605	7.0	0.236	1.0	4.0	8.0
Mg-SiO_2	547	2.2	0.166	0.2	3.7	8.0

Table 5-4. SOLAR-CELL PERFORMANCE FOR FRONT- AND BACK-ILLUMINATED a-Si:H p-i-n CELLS

Back Electrode	Illumination	V_{oc} (mV)	J_{sc} (mA/cm^2)	FF	η (%)
Ti	Front, AM1	809	4.79	0.57	2.2
ITO	Front, AM1	843	3.63	0.355	1.1
ITO	Back, AM1	862	7.29	0.282	1.8
ITO	Back, 0.55 AM1	848	3.08	0.352	2.1

The large increase in J_{sc} and η for the back illumination vs front illumination is most likely due to more light getting through to the active region. The fact that the voltages remain unimpaired is very encouraging.

The differences between the current and efficiency for front-illuminated cells having the Ti and ITO back electrodes are due to the combination of the sheet resistivities and the reflectivities of the back electrodes.

5.1.7 Effect of T_s and rf Power on Dopant Concentration

In our recent Final Report [2], we reported an improvement in solar-cell performance with decreasing rf deposition power. Dependence of the conductivity of doped layers on rf power and T_s was reported as well. We designed an experiment to measure the doping concentration as a function of rf power and T_s as follows: A boron-doped and a phosphorus-doped film were deposited on different glass substrates having a temperature gradient from 180 to 325°C along the film and seven levels of variations of rf power in the vertical direction from 0.03 to 0.9 W/cm^2. The dopant ratios B_2H_6/SiH_4 and PH_3/SiH_4 were kept constant and had values of 5×10^{-3} and 3×10^{-3}, respectively. The dopant gases were admixed from 1% mixtures in H_2.

SIMS depth profile analysis was made of the boron-doped sample. It showed that boron concentration varied inversely with rf power by about a factor of 2 and also inversely with T_s. The average [B] concentration was 0.4% at 325°C and 0.6% at 180°C. The increase in [B] concentration with decreasing rf power is consistent with the increased photoconductivity and better solar-cell performance reported previously.

The analysis for phosphorus was done by Auger depth profile analysis. The phosphorus concentration varied inversely with the rf power from ~0.45 to 0.15% P over the given range. In contrast to the boron-doped sample, there was no variation in P content with temperature.

As reported earlier, the dark conductivity of phosphorus-doped samples decreases by a factor of 10^3 for samples deposited at low rf power (0.06 W/cm^2), although they have a higher P content. Apparently the manner in which the incorporation of phosphorus takes place varies with the rf power level.

5.1.8 Dependence of the Quantum Efficiency of i-n and p-i-n a-Si:H Solar Cells

Published data for the quantum efficiency (QE) or collection efficiency of i-n and p-i-n a-Si:H solar cells indicate that the latter show an inferior response at short wavelengths (blue and green light). The reason for this is the strong absorption of the light by the p layer, coupled with the fact that the recombination lifetime in the p layer is very short - hence any electron-hole pairs generated in this layer do not contribute to the photocurrent. Yet the p layer is desirable because it increases the V_{oc} of the cell significantly (compare data in Figs. 5-2 and 5-7 and in Table 5-2).

To obtain experimental data on the dependence of the QE on the thickness of the p layer we determined the QE of the sample described in the caption of Fig. 5-2, at different p layer thicknesses and constant i- and n-layer thicknesses. These data appear in Fig. 5-13, showing the expected progressive decrease of QE at high p-layer thicknesses.

Similarly we determined the QE dependence on the thickness of the i layer for i-n cells having graded i- and n-layer thicknesses (cell described in the caption for Fig. 5-7). The data were taken for increasing i-layer thicknesses and constant n-layer thickness. As shown in Fig. 5-14, we see approximately a constant value of QE at $\lambda = 0.4$ μm, whereas between $\lambda = 0.5$ and 0.7 μm the QE increases with i-layer thickness due to the fact that more of the longer-wavelength radiation is absorbed and converted to photocurrent. Maximum QE would be expected at an i-layer thickness equal to or greater than the depletion width.

The QE curves will be all-important as a diagnostic tool in the optimization of the structure of a-Si:H solar cells (see Section 6.1).

5.2 SOLAR CELLS OF a-(Si,Ge):H ALLOYS

As a part of the program of developing improved stacked cells we made p-i-n cells similar to our a-Si:H cells but substituted various amounts of Ge for Si, using GeH_4 as a source. Precipitous decreases of cell performance took place within the first 10% of GeH_4 in the gas mixture. A cell made from pure a-Ge:H did not form a diode. The dependencies of V_{oc} and J_{sc} on T_s and Ge concentration are shown in Figs. 5-15 and 5-16, respectively.

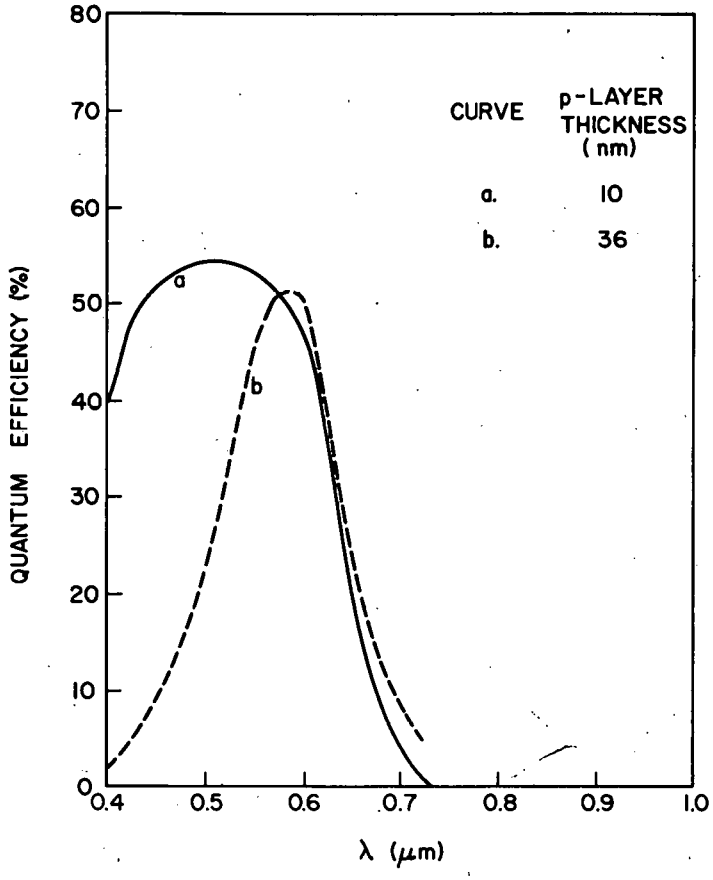

Figure 5-13. THE DEPENDENCE OF THE SPECTRAL RESPONSE OF p-i-n a-Si:H SOLAR CELLS ON THE p-LAYER THICKNESS

A plot of V_{oc} and J_{sc} vs Ge content at constant T_s of 210°C reveals that V_{oc} decreases approximately linearly, whereas J_{sc} decreases experimentally.

The tentative conclusion at this point is similar to that found by D. E. Carlson [21], namely, that Ge in a-Si:H cells acts as a detrimental impurity. It will not be suitable for use in stacked cells.

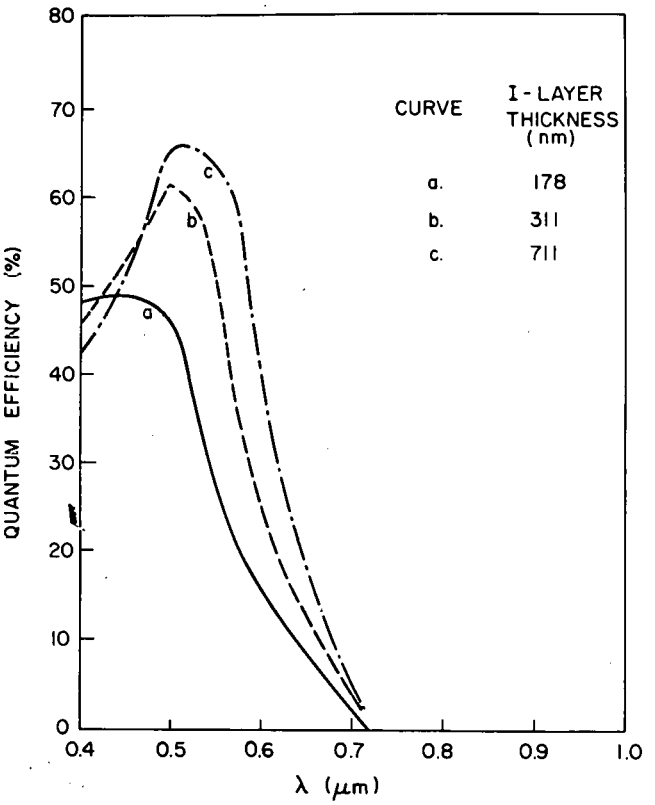

Figure 5-14. THE DEPENDENCE OF THE SPECTRAL RESPONSE OF i-n a-Si:H SOLAR CELLS (DESCRIBED IN THE CAPTION FOR FIG. 5-7) ON THE i-LAYER THICKNESS

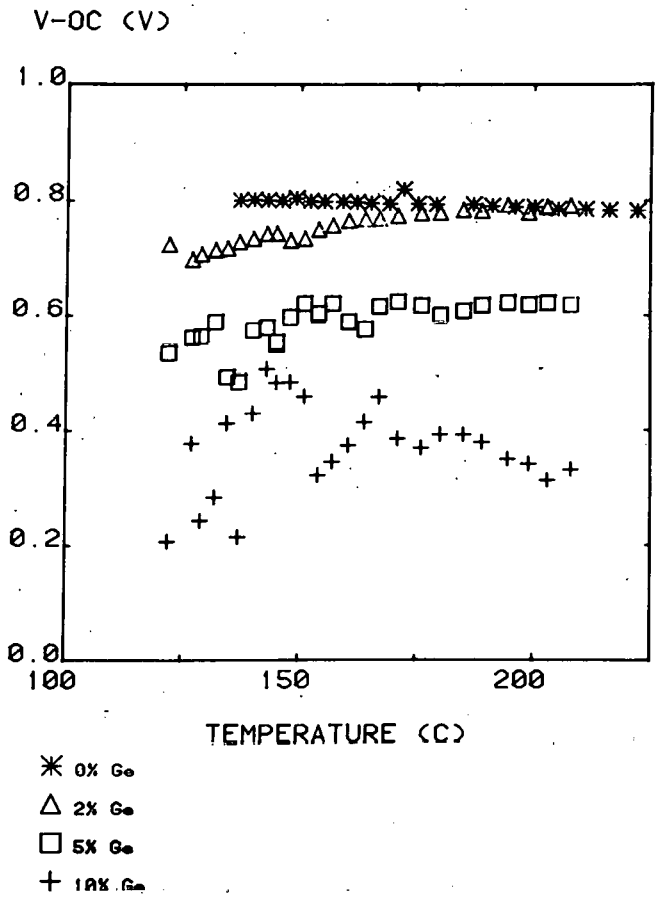

Figure 5-15. THE DEPENDENCE OF V_{oc} ON THE DEPOSITION TEMPERATURE AND THE Ge CONTENT [$GeH_4/(GeH_4 + SiH_4)$] OF SOLAR CELLS OF a-(Si,Ge):H

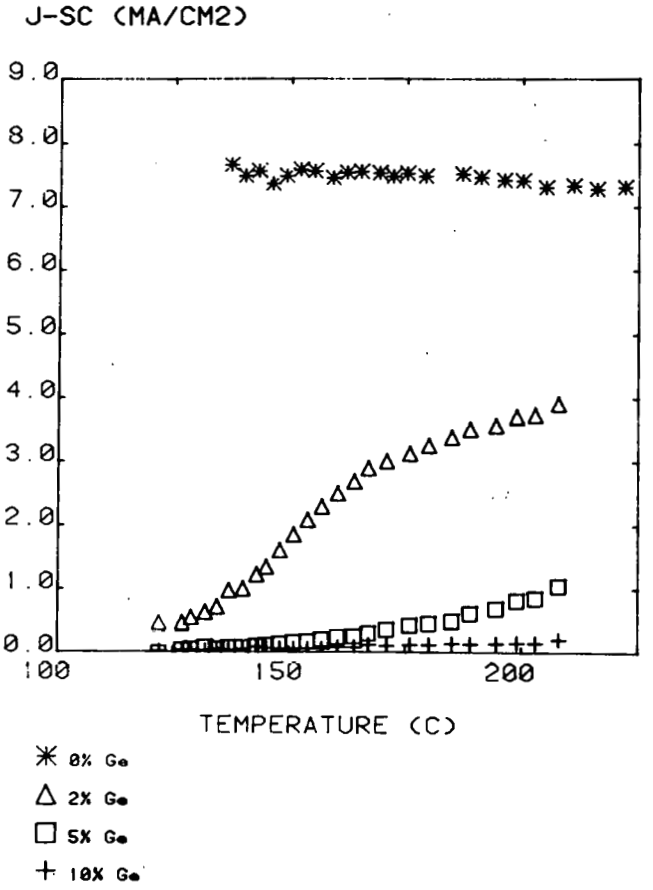

Figure 5-16. THE DEPENDENCE OF J_{sc} ON THE DEPOSITION TEMPERATURE AND THE Ge CONTENT [$GeH_4/(GeH_4 + SiH_4)$] OF SOLAR CELLS OF a-(Si,Ge):H

THIS PAGE

WAS INTENTIONALLY

LEFT BLANK

SECTION 6.0

THEORETICAL AND EXPERIMENTAL EVALUATION OF SOLAR-CELL PARAMETERS

6.1 THE SPECTRAL RESPONSE OF a-Si:H SOLAR CELLS

The factors limiting the short-circuit current density of a solar cell can often be identified by studying the collection efficiency (or quantum efficiency) response of the cell. If the cell is not limited by a large series resistance or a small shunt resistance, then J_{sc} can be directly related to the cell's spectral response or collection efficiency, $\eta_{coll.}(\lambda)$:

$$J_{sc} = q\int F(\lambda)\ \eta_{coll.}(\lambda)\ d\lambda \qquad (6\text{-}1)$$

where $F(\lambda)$ is the solar irradiance and λ is the wavelength of light.

The spectral response of a-Si:H solar cells can vary significantly depending on both the deposition conditions and the structure of the cell. Figure 6-1 shows the spectral response of three different solar-cell structures. Curve (A) is the response of an ITO/i-n structure, and curve (B) shows the response of the same cell after a reverse bias of 0.5 V was applied. Curve (C) is the response of an ITO/n-i-p structure, and curve (D) that of a glass/ITO/cermet/i-n structure. The measured short-circuit current densities for each cell are shown in parentheses. The data in Fig. 6-1 were obtained with a monochromator at low light levels ($\sim 10^{-3}$ AM1). Recent results have shown that the response of some a-Si:H solar cells can change appreciably as the light intensity increases (see Fig. 6-2).

The collection efficiency as a function of wavelength, $\eta_{coll.}(\lambda)$, should be measured with a chopped monochromatic light beam in the presence of steady AM1 illumination. There are several mechanisms that can change $\eta_{coll.}(\lambda)$ with light intensity: (1) the width of the collection region can decrease significantly in some a-Si:H cells due to the trapping of photogenated holes in the depletion region; (2) some traps and recombination centers can be saturated at high light levels; (3) field-dependent recombination can be affected by both a change in the depletion width and a change in the built-in potential due to the changing photoconductivity of a quasi-neutral region; and (4) the photocurrent at short wavelengths may be limited by the resistance of the quasi-neutral region.

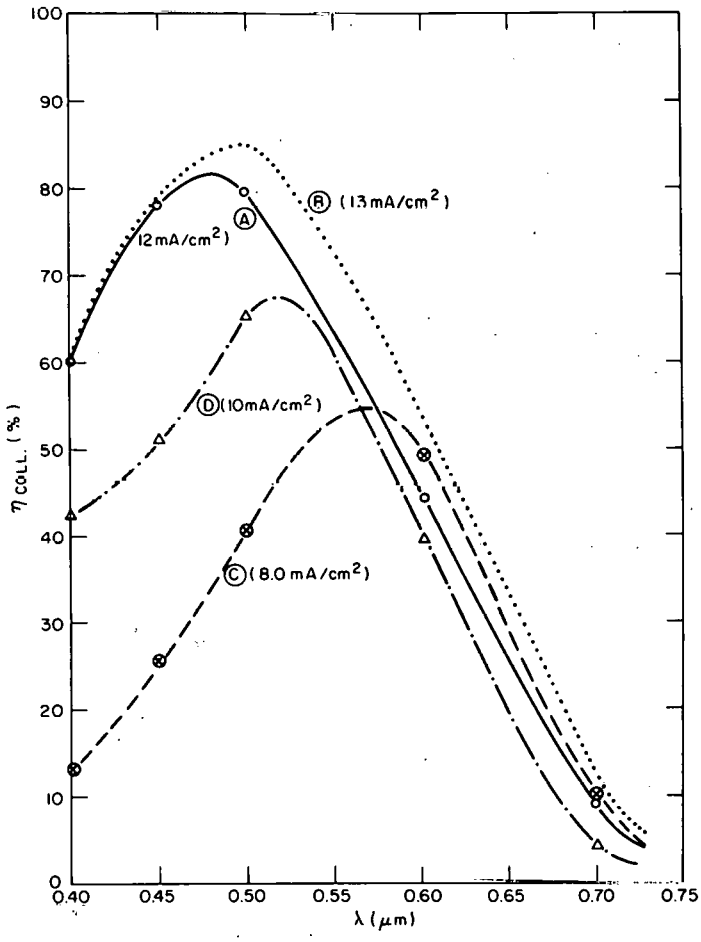

Figure 6-1. COLLECTION EFFICIENCY AS A FUNCTION OF λ FOR (A) AN ITO/i-n STRUCTURE (active area ~ 2.6 cm^2), (B) THE SAME CELL UNDER -0.5 V BIAS, (C) AN ITO/n-i-p structure (active area ~ 1.1 cm^2), AND (D) A GLASS/ITO/CERMET/i-n STRUCTURE (active area ~ 2.5 mm^2). The measured values of J_{sc} are shown in parentheses.

Now we would like to consider what effect the doped layers in p-i-n cells would have on the spectral response. If the doping levels are on the order of 1 at. %, then the recombination lifetimes are apparently very short, and very few carriers would be collected from the doped layers (both photoconductivity [22] and photoluminescence [23] are reduced significantly at these doping levels).

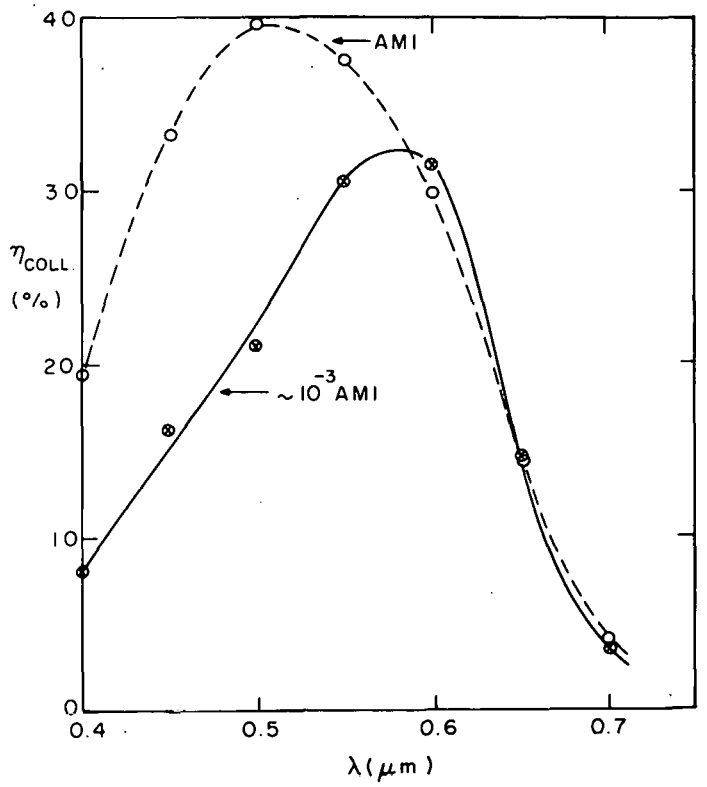

Figure 6-2. COLLECTION EFFICIENCY AS A FUNCTION OF λ FOR A p-i-n CELL MEASURED AT LOW LIGHT LEVELS ($\sim 10^{-3}$ AM1) AND AT ~AM1 ILLUMINATION.

Figure 6-3 shows some optical absorption data for films grown in rf electrodeless discharge at $T_s \simeq 330°C$ (the hydrogen content was ~25 at. %). Use of these data enables us to calculate the upper limits for $\eta_{coll.}(\lambda)$ by assuming that all photons absorbed in a doped layer are lost, while those absorbed in the undoped layer lead to collected electron-hole pairs. For a heterojunction, Schottky-barrier, or MIS cell, we assume an optical path length of 1 μm (e.g., a 0.5-μm-thick, fully depleted cell with a reflective substrate) and ignore other loss mechanisms (such as reflection losses, absorption in the top contacting layer, and recombination in the depletion region). The calculated $\eta_{coll.}(\lambda)$ curve is labeled "no n layer" in Fig. 6-4. Using the solar irradiance curve, $F(\lambda)$, shown in Fig. 6-4, we can use Eq. 6-1 to calculate J_{sc}. This value of 17.9 mA/cm^2 will increase as the optical absorption of the a-Si:H film increases (by decreasing the hydrogen content).

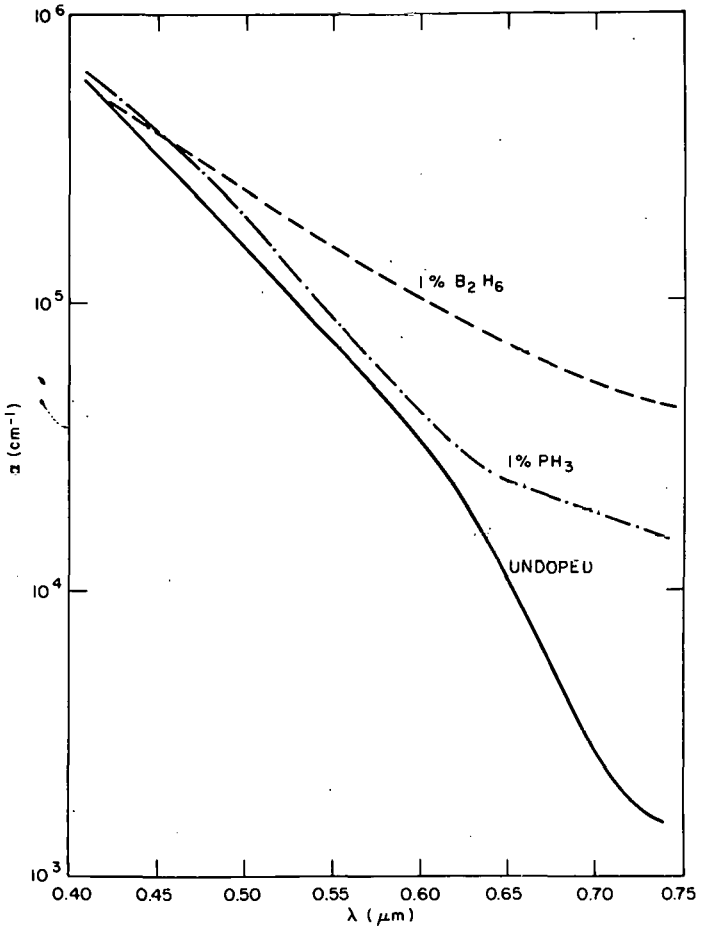

Figure 6-3. THE ABSORPTION COEFFICIENTS AS A FUNCTION OF WAVELENGTH FOR DOPED AND UNDOPED a-Si:H

If we now place a 10-nm-thick layer of n-type material on top of the undoped a-Si:H and assume that the n layer is dead, then we obtain a spectral response curve with significantly lower response at short wavelengths (see Fig. 6-4).

$$\eta_{coll.} = \ell^{-\alpha_n d_n} (1 - \ell^{-2\alpha_1 d_i}) \qquad (6\text{-}2)$$

where α_n and α_i are the optical absorption coefficients and d_n and d_i are the thicknesses of the doped and undoped layers, respectively. When the thickness of the n layer is increased to 40 nm, an even larger decrease occurs in the short-wavelength response and a small shift in the peak to longer wavelengths is observed.

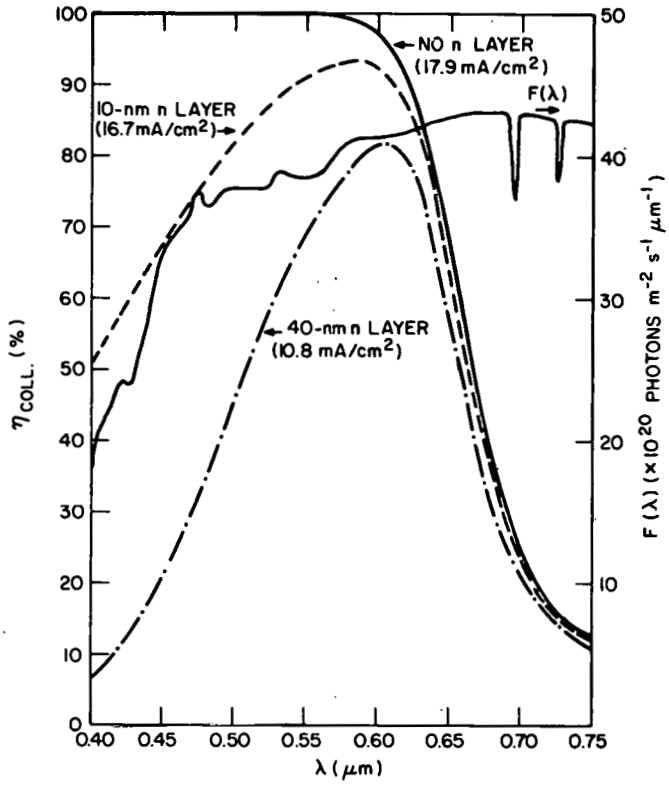

Figure 6-4. CALCULATED COLLECTION EFFICIENCIES AS A FUNCTION OF WAVELENGTH FOR NO-TOP-DOPED LAYER AND FOR TWO THICKNESSES OF A TOP n LAYER. The solar irradiance for AM1 illumination is also shown.

In Fig. 6-5, we show similar spectral response curves for dead p layers (10 nm and 40 nm thick). Since the absorption in the p-type material is greater than that in the n-type material for most wavelengths (see Fig. 6-3), J_{sc} is reduced by greater amounts; thus a 40 nm p layer reduces J_{sc} by ~50%, while a 40 nm n layer reduces J_{sc} by only ~40% (see Fig. 6-4).

In the next few months, we will perform detailed analyses of our best cells to include all known loss mechanisms. We will then use this modeling to define those areas where device performance can be most readily improved.

6.2 SPECTRAL DEPENDENCE OF THE MAJORITY-CARRIER GAIN IN n-TYPE a-Si:H SOLAR CELLS

The spectral dependence of the majority-carrier photocurrent is often used to probe for optically active defects in insulators and semiconductors. This

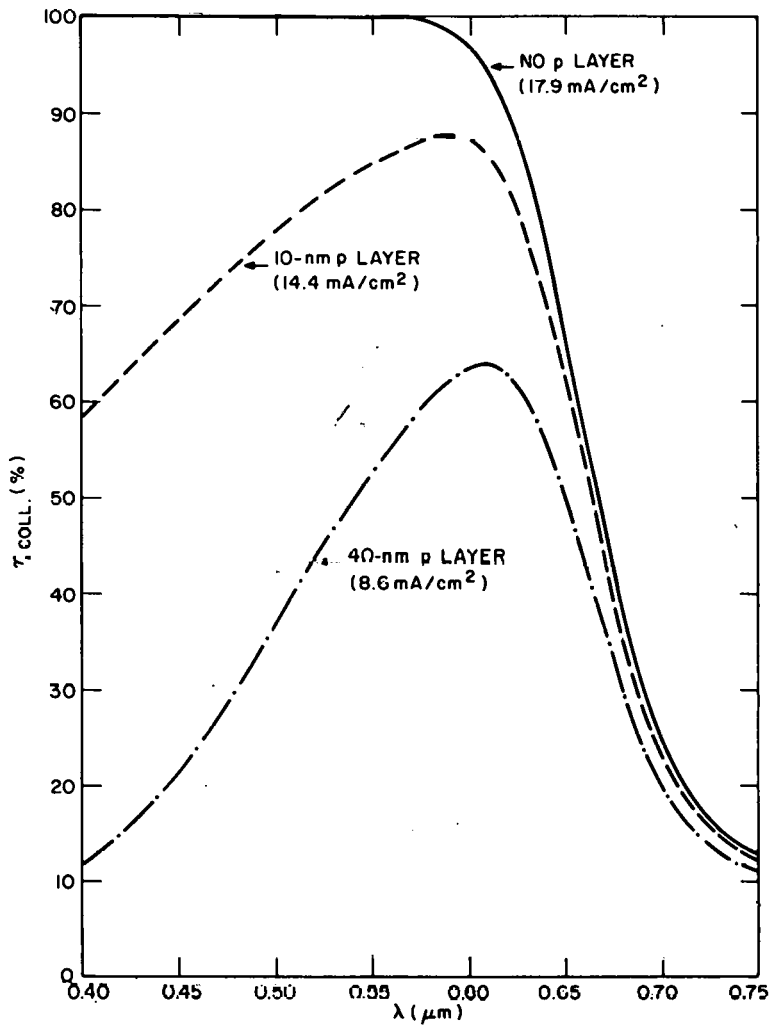

Figure 6-5. CALCULATED COLLECTION EFFICIENCIES AS A FUNCTION OF WAVELENGTH FOR NO-TOP-DOPED LAYER AND FOR TWO THICKNESSES OF A TOP p LAYER

technique was originally used by LeComber et al. [24] to detect gap states in hydrogenated amorphous silicon (a-Si:H). Because of their low density, these states are difficult to observe in optical absorption. The results of photoconductivity measurements have been frequently used [25-28] as a measure of gap-state density in a-Si:H. The usual assumptions are that light excites electrons into conducting states; that mobility and lifetime are independent of excitation wavelength; and that photocurrent is proportional to the number of absorbed photons and thus to the absorption coefficient. This, in turn, is assumed to be a measure of the gap-state density.

We wish to point out that photocurrent measurements can give misleading information about the gap-state density. The reason is that the electron lifetime (τ) is not independent of excitation wavelength [28]. It increases with decreasing photon energy below about 1.3 eV. It is this increase in τ that produces a peak in the photocurrent near 1.1 eV and not a peak in the gap-state density as previously assumed [26,27].

To exclude variations in τ from a photocurrent measurement one must measure the photocurrent by means of blocking contacts. In this case the current is a primary photocurrent (J_p) [29] that is proportional to the number of ionized electron-hole pairs per cm^2 per second (N_A). The high field or saturated value of J_p is

$$J_p = eN_A \quad . \tag{6-3}$$

Equation (6-3) is valid if the electric field is high enough to ensure that an electron traverses the sample without significant recombination [30]. In an a-Si:H solar-cell structure, the steady-state reverse-bias current is a primary photocurrent consisting of an equal number of electrons and holes, which for high-enough bias obeys Eq. 6-3. This current can therefore be used as a measure of the number of absorbed photons [28].

However, what has been measured usually [24-27] is the secondary photocurrent (J_s) [29]. In this case the contacts are ohmic and the current is

$$J_s = eN_A\eta \frac{\tau}{\ell} \mu E = eN_A\eta g \quad , \tag{6-4}$$

where μ is the mobility, E the field, and ℓ the sample thickness. The gain (g) is the ratio of recombination time (τ) to transit time ($\ell/\mu E$). The quantity (η) is the quantum efficiency for free-carrier production. Only if g is independent of wavelength can J_s be a measure of the density of gap states. Usually N_A is determined by measuring the reflectivity and absorption coefficient and by assuming that the quantum efficiency for free-carrier production is unity. Since it is usually difficult to determine these parameters, it is much easier to determine N_A from a measurement of the reverse-bias primary photocurrent.

Solar-cell structures are ideally suited for a measurement of both J_p and J_s. By measuring J_p and J_s in the same structure, g and N_A can be readily determined.

Under normal operating conditions a solar cell is a primary photocurrent device because in reverse bias the contacts are blocking for both electrons and holes. Forward-biasing the solar cell past the flat-band voltage (V_F) makes the cell a secondary photocurrent device. In an a-Si:H Schottky-barrier device the n contact injects electrons. In this structure the metal barrier is a blocking contact for holes. Thus, J_s is a pure electron current. In practice one measures J_p at large-enough reverse bias where the current is independent of bias. This ensures that the electron-hole recombination is insignificant and that the quantum efficiency for electron-hole ionization is not reduced below unity by geminate recombination [31]. To measure J_s, the solar cell is forward biased far enough so that η is about unity.

Photocurrent measurements were made on a solar-cell structure constructed from a-Si:H produced by glow-discharge decomposition of silane on a molybdenum-coated glass substrate. The first few hundred angstroms next to the molybdenum are phosphorus-doped a-Si:H. The next 0.5 μm is undoped a-Si:H. On top of this, a 50-Å platinum film makes the Schottky-barrier contact through which the light enters the film. A monochromator was used as a light source. The light was chopped at low frequency. The primary photocurrent was measured with a phase-sensitive detector. Because the response time of the secondary photocurrent is longer than one second, an electrometer was used to measure J_s.

In Fig. 6-6 the photocurrent is plotted vs applied voltage for an excitation wavelength of 0.83 μm. The general features of this data were also observed at other wavelengths above or below the bandgap. In the figure, positive currents are primary photocurrents; negative currents are secondary ones. The important feature is that the primary photocurrent saturates in reverse bias. This means that all the excited electron-hole pairs are collected. In other words, both electrons and holes are transported through the a-Si:H film without significant recombination.

The values of J_s and J_p, measured at 2 V and -2 V, respectively, above and below V_F, are shown as a function of excitation energy in Fig. 6-7. V_F is the voltage at which the current changes from primary to secondary. The photocurrent changes sign at this voltage.

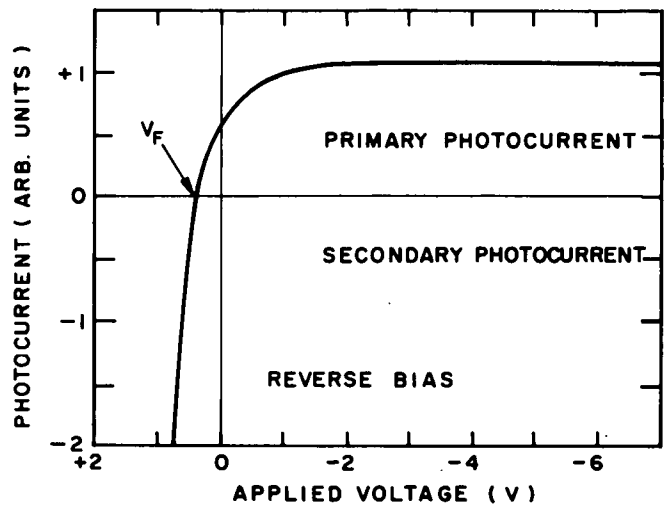

Figure 6-6. PHOTOCURRENT VS VOLTAGE APPLIED TO A SCHOTTKY-BARRIER a-Si:H SOLAR CELL. The polarity is that of the barrier contact. The photon energy is 1.49 eV. Negative voltage is reverse bias. Positive currents are primary photocurrents. The undoped-film thickness is 0.6 μm.

The secondary or ohmic photocurrent shows a small peak around 1 eV. This type of spectral variation is observed in other films prepared by either dc or rf discharge. However, this peak is not always at the same energy and in some cases a shoulder instead of a distinct maximum is observed. It is this general type of spectral dependence of J_s that is often reported [24-27]. If one were to conclude that J_s represents the spectral dependence of N_A and hence is a measure of the gap-state density, the conclusion would be that there is a peak in the gap-state density. This conclusion has been reached by various authors [25-27]. However, as is shown by the curve for J_p in Fig. 6-7, the structure in J_s is not accompanied by structure in J_p. In fact, there is little structure in J_p. Therefore, the structure in J_s is due to variations in g and not N_A. This is clearly shown in the figure where g is plotted.

The spectral dependence of g could be caused by a variation in either the electron mobility or lifetime. Measurements of the electron drift mobility [28]

show it to be independent of excitation energy throughout the region of strong gain variation (see Fig. 6-7). Measurements of the photo-Hall effect have been made by J. Dresner on a-Si:H films prepared in the same way as the ones used for the solar-cell structures (see Section 4.5). He found the photo-Hall mobility to be independent of wavelength for excitation above or below the absorption edge. Thus we are led to conclude that the gain variation is due to variations in τ with excitation energy. This result is plausible because the photo excitation process excites electrons from states above the valence band to states in or near the onduction band [28]. As the excitation energy is increased, holes that can recombine with electrons are produced in states increasingly distant above the valence band. The states farther away from the valence band decrease in number [28] and become more localized. Both these effects would be expected to decrease the electron-hole recombination probability and hence increase the electron lifetime.

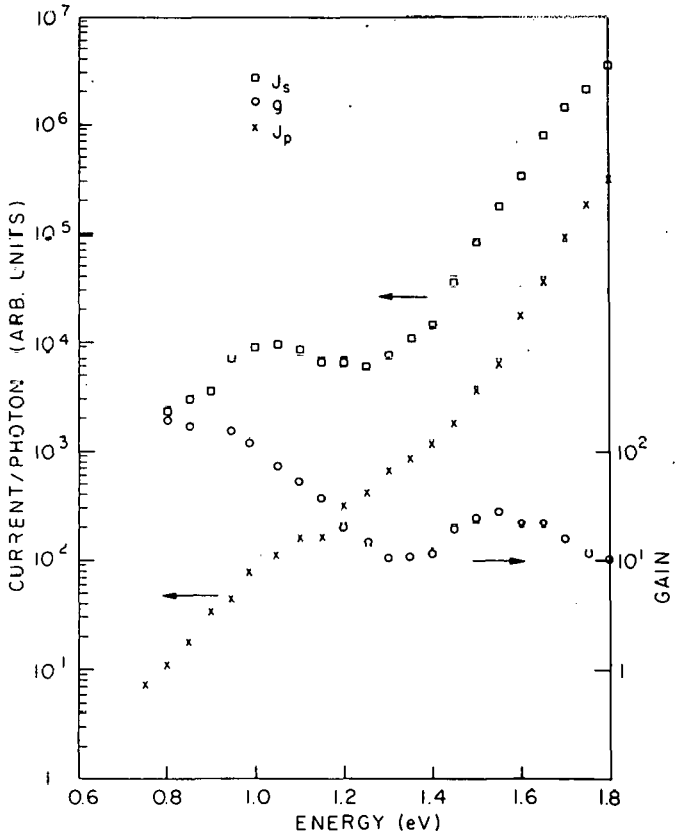

Figure 6-7. SPECTRAL DEPENDENCE OF PRIMARY (J_p) AND SECONDARY (J_s) PHOTOCURRENTS MEASURED ON AN a-Si:H SOLAR-CELL STRUCTURE AT ROOM TEMPERATURE. The gain g is the ratio of J_s to J_p.

SECTION 7.0

REFERENCES

1. D. E. Carlson, R. S. Crandall, B. Goldstein, J. J. Hanak, A. R. Moore, J. I. Pankove, and D. L. Staebler, Final Report, SAN-1286-8, prepared for Department of Energy under Contract No. EY-76-C-03-1286, Oct. 1978.
2. D. E. Carlson, I. Balberg, R. S. Crandall, B. Goldstein, J. J. Hanak, J. I. Pankove, D. L. Staebler, H. A. Weakliem, and R. Williams, Final Report, ET/21074-4, prepared for Department of Energy under Contract No. AC03-78-ET-21074, Nov. 1979.
3. W. E. Spear, J. Non-Cryst. Solids 1, 197 (1969).
4. A. Many and G. Rakavy, Phys. Rev. 126, 1980 (1962).
5. S. M. Sze, Physics of Semiconductor Devices (Wiley-Interscience, New York, 1969), p. 370.
6. P. G. LeComber and W. E. Spear, Phys. Rev. Letters 25, 509 (1970).
7. A. R. Moore, Appl. Phys. Lett. 31, 762 (1977).
8. J. I. Pankove and D. E. Carlson, Appl. Phys. Lett. 31, 450 (1977).
9. C. W. White, W. H. Christie, B. R. Appleton, S. R. Rosen, P. P. Pronko, and C. W. Magee, Appl. Phys. Lett. 33, 662 (1978); C. P. Wu and C. W. Magee, Appl. Phys. Lett. 34, 737 (1979).
10. S. S. Lau, W. F. Tseng, M. A. Nicolet, J. W. Meyer, R. C. Eckardt, and R. J. Wagner, Appl. Phys. Lett. 33, 130 (1978); J. C. Bean, H. J. Leamy, J. M. Poate, G. A. Rozgonyi, P. T. Sheng, J. S. Williams, and G. K. Celler, Appl. Phys. Lett. 33, 227 (1978); H. Nakashima, Y. Shiraki, and M. Miyao, J. Appl. Phys. 50, 5966 (1979).
11. D. E. Carlson, I. Balberg, R. S. Crandall, B. Goldstein, J. J. Hanak, J. I. Pankove, D. L. Staebler, and R. Williams, Quarterly Report No. 1, SAN-2219-1, prepared for Department of Energy under Contract No. ET78-C-03-2219, Jan. 1979, p. 42.
12. K. Weiser, Comments Solid State Phys. 6, 81 (1975).
13. P. G. LeComber, A. Madan, and W. E. Spear, J. Non-Cryst. Solids 11, (1972).
14. P. G. LeComber, D. I. Jones, and W. E. Spear, Philos. Mag. 35, 1173 (1977).
15. P. G. LeComber, W. E. Spear, and D. Allan, J. Non-Cryst. Solids 32, 1 (1979).
16. R. A. Bube, Photoconductivity of Solids (John Wiley & Sons, Inc., New York, 1960), p. 68 ff.

17. W. Beyer, H. Mell, and H. Overhof, Proc. 7th Int. Conf. Amorphous and Liquid Semiconductors, Edinburgh, Scotland, 1977.
18. W. Beyer, R. Fischer, and H. Wagner, J. Electronic Materials 8, 127 (1979).
19. W. Beyer, R. Fischer, and H. Overhof, Philos. Mag. B39, 205 (1979).
20. L. Friedman, Philos. Mag. 38, 467 (1978); J. Non-Cryst. Solids 6, 329 (1971).
21. D. E. Carlson, Tech. Dig. 1977 IEDM, Washington, DC (IEEE, New York, 1977), p. 214.
22. D. A. Anderson and W. E. Spear, Philos. Mag. 36, 695 (1977).
23. J. I. Pankove and D. E. Carlson, Appl. Phys. Lett. 29, 620 (1976).
24. P. G. LeComber, A. Madan, and W. E. Spear, in P. G. LeComber and J. Mort (eds.), Electronic and Structural Properties of Amorphous Semiconductors (Academic Press, New York, 1973), p. 373
25. P. J. Zanzucchi, C. R. Wronski, and D. E. Carlson, J. Appl. Phys. 48, 5227 (1977); T. Suzuki, M. Hirose, S. Ogose, and Y. Osaka, Phys. Status Solidi A 42, 337 (1977).
26. D. A. Anderson, G. Moddel, R. W. Collins, and W. Paul, paper presented at 8th Int. Conf. Liquid and Amorphous Semiconductors, Cambridge, MA (1979).
27. J. I. Pankove, F. J. Pollack, and C. Schnabolk, paper presented at 8th Int. Conf. Liquid and Amorphous Semiconductors, Cambridge, MA (1979).
28. R. S. Crandall, paper presented at 8th Int. Conf. Liquid and Amorphous Semiconductors, Cambridge, MA (1979).
29. A. Rose, RCA Rev. 12, 362 (1951).
30. K. Hecht, Z. Physik 77, 235 (1932).
31. R. S. Crandall, R. Williams, and B. E. Tompkins, J. Appl. Phys. 50, 5506 (1979).

*U.S. GOVERNMENT PRINTING OFFICE:1980 740-145/533